

Ionic Hubbard model on a triangular lattice for $\text{Na}_{0.5}\text{CoO}_2$, $\text{Rb}_{0.5}\text{CoO}_2$ and $\text{K}_{0.5}\text{CoO}_2$: Mean-field slave boson theory

B. J. Powell,^{1,*} J. Merino,² and Ross H. McKenzie¹

¹*Centre for Organic Photonics and Electronics, School of Mathematics and Physics,
The University of Queensland, Brisbane, Queensland 4072, Australia*

²*Departamento de Física Teórica de la Materia Condensada,
Universidad Autónoma de Madrid, Madrid 28049, Spain*

We introduce a strongly correlated mean-field theory of the ionic Hubbard model on the triangular lattice with alternating stripes of site energy using Barnes-Coleman slave bosons. We study the paramagnetic phases of this theory at three quarters filling, where it is a model of $\text{Na}_{0.5}\text{CoO}_2$, $\text{Rb}_{0.5}\text{CoO}_2$, and $\text{K}_{0.5}\text{CoO}_2$. This theory has two bands of fermionic quasi-particles: one of which is filled or nearly filled and hence weakly correlated; the other is half-filled or nearly half-filled and hence strongly correlated. Further results depend strongly on the sign of the hopping integral, t . The light band is always filled for $t > 0$, but only becomes filled for $|\Delta/t| \geq 1.5$ for $t < 0$, where Δ is the difference in the site energies of the two sublattices. A metal-charge transfer insulator transition occurs at $|\Delta/t| = 5.0$ for $t > 0$ and $|\Delta/t| = 8.0$ for $t < 0$. In the charge transfer insulator complete charge disproportionation occurs: one sublattice is filled and the other is half filled. We compare our results with exact diagonalisation calculations and experiments on $\text{Na}_{0.5}\text{CoO}_2$, and discuss the relevance of our results to $\text{Rb}_{0.5}\text{CoO}_2$ and $\text{K}_{0.5}\text{CoO}_2$. We propose a resolution of seemingly contradictory experimental results on $\text{Na}_{0.5}\text{CoO}_2$. Many experiments suggest that there is a charge gap, yet quantum oscillations are observed suggesting the existence of quasiparticle states at arbitrarily low excitation energies. We argue that the heavy band is gapped while the light band, which contains less than 1 charge carrier per 100 unit cells, remains ungapped.

PACS numbers:

I. INTRODUCTION

Experiments on $A_x\text{CoO}_2$, where A is Na, Rb, or K, show a wide range of strongly correlated phases.^{1,2} $\text{Na}_{0.5}\text{CoO}_2$, in particular, has attracted much attention following the discovery of superconductivity when water is intercalated into the system.³ The phase diagram, with doping x , shows many interesting phases,^{1,2,4} including a ‘Curie-Weiss metal’, A type antiferromagnetism (ferromagnetic layers stacked antiferromagnetically) and an ‘insulating’ phase seen only at $x = 0.5$. The latter phase is particularly puzzling as many probes [including resistivity,⁴ optical conductivity,⁵ and angle resolved photoemission spectroscopy (ARPES)⁶] suggest that it is insulating, however, Shubnikov-de Haas oscillations are also observed,⁷ suggesting the state is metallic. The aims of this paper are to present a simple variational theory of $A_{0.5}\text{CoO}_2$, where $A=\text{Na, Rb, or K}$, and to attempt to reconcile these seemingly contradictory experiments.

In $A_x\text{CoO}_2$ the Co atoms form a triangular lattice and the simplest model of the band structure, a single band triangular lattice with nearest neighbour hopping only, gives good agreement with ARPES experiments on Na_xCoO_2 .⁸ The doping of the system is controlled by the concentration of A ions, x , with the single band being half filled at $x = 0$ and filled at $x = 1$. However, the A ions order so as to minimise the mutual Coulomb repulsion.^{9,10,11} Therefore, the Coulomb potential due to the A ions is different at different Co atoms and, because the A ions are ordered, this gives rise to an ordered arrangement of potentials at the vertices of the triangular

lattice. Thus an effective Hamiltonian for $A_x\text{CoO}_2$ is the ionic Hubbard model.²

In addition to the interest in $A_x\text{CoO}_2$ the ionic Hubbard model is of significant interest in its own right. The ionic Hubbard model on half filled bipartite lattices has attracted interest because it undergoes a transition from a Mott insulator to a band insulator.^{12,13,14,15,16,17,18} Furthermore, away from half filling and on frustrated lattices the ionic Hubbard model shows a subtle interplay between charge and spin ordering and metallic and insulating phases.^{19,20,21,22,23,24} The Hamiltonian of the ionic Hubbard model is

$$\hat{\mathcal{H}} = -t \sum_{\langle ij \rangle \sigma} \hat{c}_{i\sigma}^\dagger \hat{c}_{j\sigma} + U \sum_i \hat{n}_{i\uparrow} \hat{n}_{i\downarrow} + \sum_i \epsilon_i \hat{n}_{i\sigma}, \quad (1)$$

where t is the hopping amplitude between nearest neighbour sites only, U is the effective on-site Coulomb repulsion between two electrons, ϵ_i is the site energy, $\hat{c}_{i\sigma}^{(\dagger)}$ annihilates (creates) an electron on site i with spin σ and $\hat{n}_{i\sigma} = \hat{c}_{i\sigma}^\dagger \hat{c}_{i\sigma}$. Previous studies of this model on frustrated lattices included both analytical and numerical studies of zigzag ladders,^{19,20} dynamical mean field theory (DMFT) studies on infinite dimensional fcc²¹ and two-dimensional triangular lattices²² and exact diagonalisation on small triangular lattices.^{23,24} A more extensive discussion of previous work on the ionic Hubbard model is given in Ref. 24. However, here we aim to provide a simple variational description that captures as much of the strongly correlated physics of this model as possible.

The wide range of numerical techniques, described above, that have been applied to the ionic Hubbard

model have not, previously, been complemented by a commensurate effort to develop simple variational approaches. The history of the theory of strongly correlated electrons shows that progress has often been made when accurate numerical techniques are combined with such variational calculations. Therefore, our theory, which can be straightforwardly generalised to other potential arrangements, lattices, fillings, etc., is complementary to the previous numerical work.

In Na_xCoO_2 many different Na ordering patterns are seen at different values of x ,^{9,10,11} and each of these correspond to a different $\{\epsilon_i\}$.² In principle, each of these different $\{\epsilon_i\}$ correspond to a different Hamiltonian. Therefore, for simplicity and definiteness, we specialise to the Hamiltonian relevant to $x = 0.5$. This model has two sublattices with different site energies, $\epsilon_i = \Delta/2$ for A-sites and $\epsilon_i = -\Delta/2$ for B-sites,² and with the sublattices arranged in stripes as shown in Fig. 1b. Thus the Hamiltonian is

$$\hat{\mathcal{H}} = -t \sum_{\langle ij\alpha\beta \rangle \sigma} (\hat{c}_{i\alpha\sigma}^\dagger \hat{c}_{j\beta\sigma}) + U \sum_{i\alpha} \hat{n}_{i\alpha\uparrow} \hat{n}_{i\alpha\downarrow} + \sum_{i\sigma} \frac{\Delta}{2} (\hat{n}_{iA\sigma} - \hat{n}_{iB\sigma}), \quad (2)$$

where $\hat{c}_{i\alpha\sigma}^{(\dagger)}$ annihilates (creates) an electron with spin σ in an orbital centred on site i belonging to sublattice α and $\langle ij\alpha\beta \rangle$ indicates that the sum is over nearest neighbours on the appropriate sublattices only.

Hamiltonian (2) is a natural instance of Hamiltonian (1) for initial study on both theoretical and experimental grounds. Experimentally, the behaviour of, particularly, $\text{Na}_{0.5}\text{CoO}_2$ is very different from that of Na_xCoO_2 with x either a little larger or smaller than 0.5. Further, many of the phenomena observed at $x = 0.5$ seem to have a natural explanation in terms of the ionic Hubbard model.^{2,23,24} We have previously studied the quarter-filled ionic Hubbard model with a stripe potential by exactly diagonalising small clusters.^{23,24} We found a complicated interplay between the charge and spin degrees of freedom and between insulating and metallic states. We also found that these calculations provide a possible framework for understanding a wide variety of experiments on $\text{Na}_{0.5}\text{CoO}_2$, $\text{Rb}_{0.5}\text{CoO}_2$, and $\text{K}_{0.5}\text{CoO}_2$. However, the most interesting regime (i.e., $-t \sim \Delta \ll U$, see section IB), in terms of its relevance to experiments, is also the most challenging to investigate theoretically. This provides additional motivation to investigate the simpler mean-field theory presented below. Comparison between our mean-field theory and these exact diagonalisation calculations will be made, where possible, below.

The rest of this paper is organised as follows. In the remainder of this introduction we briefly review the most pertinent experiments on $\text{Na}_{0.5}\text{CoO}_2$ and previous theories aimed at explaining these measurements. In section II we give the formal details of our theory and derive a set of self-consistency equations for the ground state. In section III we report the results of numerical solutions

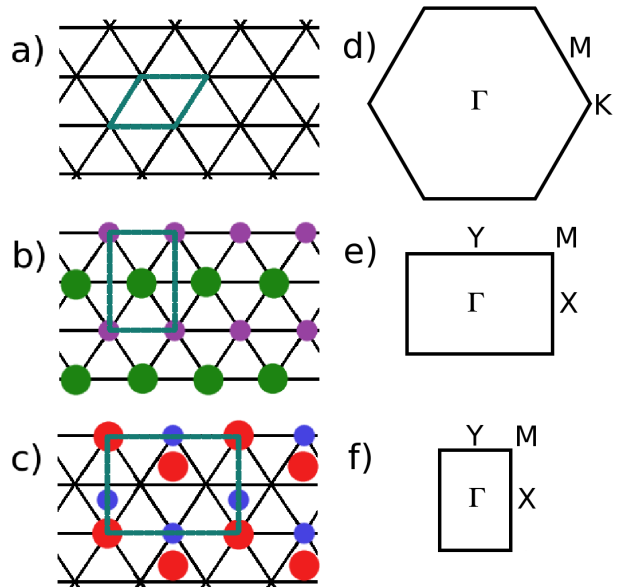


FIG. 1: [Color online] The various unit cells and Brillouin zones discussed in this paper: (a) the unit cell of the isotropic triangular lattice; (b) the unit cell of the ionic Hubbard model [Eq. (2)]; and (c) the basal plane of the unit cell of $\text{A}_{0.5}\text{CoO}_2$; panels (d), (e), and (f) show the Brillouin zones corresponding to the unit cells in panels (a), (b), and (c) respectively. In (b) the different size circles distinguish the A and B sublattices. In (c) the large red (small blue) circles indicate the positions of Na ions above (below) the CoO_2 plane. The unit cell of the ionic Hubbard model (b) is twice as large as that of the Hubbard model of the triangular lattice (a). Further note that the basal plane of the unit cell of $\text{A}_{0.5}\text{CoO}_2$ is twice as large as the unit cell of the ionic Hubbard because of the periodicity of the (out of plane) A ions. Selected high symmetry points are marked in the Brillouin zones. Note that the Brillouin zones are drawn to scale and that the Γ -point [$\mathbf{k} = (0, 0)$] is equivalent in each Brillouin zone.

of these equations and compare our results with experiments on $\text{A}_{0.5}\text{CoO}_2$ and previous theoretical studies of the triangular lattice ionic Hubbard model. In section IV we draw our conclusions. In appendix A we describe the band structure of the model (2) for non-interacting electrons.

A. Experiments on $\text{Na}_{0.5}\text{CoO}_2$

There has been far less experimental work on $\text{K}_{0.5}\text{CoO}_2$ or $\text{Rb}_{0.5}\text{CoO}_2$ than $\text{Na}_{0.5}\text{CoO}_2$. Therefore, in this section, we focus mainly on experiments on $\text{Na}_{0.5}\text{CoO}_2$. The brief review below brings out two particular puzzles that theory needs to explain about the ground state. The first is how it is some properties are consistent with a metallic ground state and that others are more consistent with an insulating ground state. The second puzzle concerns how it is that the ground state has a large magnetic moment but a small amount

of charge ordering.

1. Charge order on the cobalt ions

Measurements of the relaxation rates for ^{59}Co NMR found two distinct Co sites, consistent with a charge ordered state.²⁵ However, the authors noted that the degree of charge disproportionation is rather small. More recent ^{59}Co and ^{23}Na NMR measurements find no signature of differences in the charge state of the cobalt ions at the two distinct sites,²⁶ suggesting that all the Co atoms are in the charge state $\text{Co}^{(3.5\pm\eta)+}$, where $\eta < 0.2$ gives an upper bound on the extent of charge ordering.²⁶ This is in contrast, to the case of $x = 0.7$ or 0.75 for which NMR clearly detecting a charge disproportionation.^{34,35} High resolution neutron crystallography detects small differences in Co-O bond lengths, and an analysis based on bond valence sums, is consistent with a charge order of $\eta \simeq 0.06$.²⁷ Very recent NMR measurements were able to detect a very small charge ordering along the Co(1) chains, below 51 K,²⁸ but the authors do not discuss the magnitude of the difference in charge between two sublattices.

2. Transport properties

As the temperature decreases the intralayer resistivity increases monotonically. No feature is seen at the magnetic ordering temperature (88 K, see below). Above 51 K, it is weakly temperature dependent with values of a few $\text{m}\Omega\text{ cm}$,⁴ characteristic of a “bad” or incoherent metal which does not have well-defined quasi-particle excitations.² Below 51 K, the resistivity increases significantly, consistent with an activated form with energy gap of about 10 meV.⁴ Although, it is usually stated that the transition at 51 K is a “metal-insulator” transition, we stress that it is really above 51 K $\text{Na}_{0.5}\text{CoO}_2$ is a bad metal and below 51 K the experimental evidence is not all consistent with the claim that $\text{Na}_{0.5}\text{CoO}_2$ is an insulator (see section I A 4).

Applying hydrostatic pressure causes the resistivity to decrease and the temperature where the resistivity becomes activated to increase. Above about 13 GPa the resistivity has a metallic temperature dependence.²⁹ In contrast, for $x=0.75$ Na_xCoO_2 is metallic at ambient pressure but becomes insulating above about 23 GPa.

Resistivity measurements found that the charge gap apparent from the resistivity was suppressed by magnetic fields parallel to the layers, larger than about 35 T, with hysteresis between 15 and 40 T, at low temperatures.⁷ A field perpendicular to the layers does not suppress the “insulating” state.³⁰

The thermopower and Hall coefficient have small and weakly temperature dependent positive values above 100 K.⁴ However, they change sign near 88 K, obtain large negative values below 50 K, and then decrease towards

zero at low temperatures. The latter is distinctly different from the behaviour of conventional semiconductors and insulators, for which the thermopower and Hall constant both diverge as the carrier density vanishes with decreasing temperature.

3. Other evidence for a gap

Quasi-particle features are only observed in angle resolved photoemission spectroscopy (ARPES) below about 150 K and reveal a Fermi surface consistent with a hole-like band for a tight-binding model on the triangular lattice with an effective hopping integral of $t_{eff} \simeq -16$ meV,⁶ about six times smaller than that predicted by LDA calculations. A gap begins to open up over the Fermi surface below about 60 K, and has a magnitude of about 6-11 meV at 10 K.⁶

Measurements of the frequency dependence of the conductivity show no evidence of a Drude peak, consistent with the bad metal behaviour, seen in the static transport quantities.^{2,5} Below about 100 K there is a loss of spectral weight at frequencies below about 100 cm^{-1} , consistent with the opening of a charge gap. This leads to a peak in $\sigma(\omega)$ at $\omega \simeq 200\text{ cm}^{-1}$.⁵ In comparison for Na_xCoO_2 , with x away from 0.5, a Drude peak is present at low temperatures and the total spectral weight of the optical conductivity scales with $1 - x$.⁵

4. Evidence for a metal

Shubnikov-de Haas oscillations are observed in the field range of 15-30 T.⁷ A fast Fourier transform of the oscillatory part of the conductivity has peaks at frequencies of 150 T and 40 T. These frequencies correspond to pockets with cross-sectional areas of 0.25 % and 0.06 % of the area of the undistorted hexagonal Brillouin zone (cf. Figure 1d). The effective mass associated with these orbits are (in units of the free electron mass) 1.2 ± 0.1 and 0.6 ± 0.5 , respectively. These measurements are extremely surprising given the range of other evidence suggesting that $\text{Na}_{0.5}\text{CoO}_2$ has an insulating ground state.

5. Magnetic properties

Muon spin rotation (μSR) experiments first saw evidence for magnetic order below about 86 K, and slight effects at 50 K and 30 K.³³ Below 88 K, there is a splitting of NMR lines, consistent with the development of commensurate antiferromagnetic order.²⁶ The change in the resistivity from a bad metal to an activated behaviour at 51 K has little effect on the magnetic state. Elastic neutron scattering also detects long-range antiferromagnetic order below 88 K, with a magnetic moment of $0.26(2)\mu_B$ per magnetic cobalt ion.^{31,37} The authors interpret this order in terms of alternating rows of magnetic

Co^{3+} and non-magnetic Co^{4+} ions. (i.e., complete charge order). However, we stress that the observation of such magnetic order does not require charge ordering to be present. Simple classical arguments suggest the magnetic moment should be less than $\mu_B(n_B - n_A)/2$ where n_ν is the average number of electrons on the $\nu = A, B$ sublattice. Hence, the charge disproportionation observed in the crystallography experiments discussed above, would imply a moment of about $0.06\mu_B$, about one quarter of the observed value.

Both the bulk magnetic susceptibility and the Knight shift are weakly temperature dependent, with a peak around 300 K, and a magnitude of about 5×10^{-3} emu/mol.^{4,26} This suggests an antiferromagnetic exchange between magnetic ions of order a few hundred Kelvin.

6. Related materials

At other values of x in Na_xCoO_2 , the ordering of sodium ions has been found to be important for the existence of various ordered phases.^{34,35,36,38,39} No insulating state is seen in the corresponding misfit cobaltates,⁴⁰ which supports the claim that Na-ordering is necessary for the insulating state. Furthermore, cooling a material at different rates found that the presence of sodium ordering can drive an additional magnetic phase transition at $x = 0.8$ and 0.85 .⁴¹

B. Theories of $\text{Na}_{0.5}\text{CoO}_2$

Choy *et al.*⁴² considered an extended Hubbard model that included the Coulomb interaction between electrons on neighbouring sites, V , but neglected the Na-ordering and the ‘ionic’ term in Eq. (2). They argued that V stabilises a charge ordered state and considered an effective low-energy Hamiltonian for this charge ordered state. By fine tuning the parameters in their effective Hamiltonian Choy *et al.* were able to reproduce the observed temperature dependence of the resistivity and the Hall coefficient.

Lee *et al.*^{43,44} have studied $\text{Na}_{0.5}\text{CoO}_2$ via LDA+U calculations that allow for the effects of Na-ordering. They find a first order metal-charge ordered insulator transition as U is increased. The charge disproportionation and the opening of the gap both occur at a single phase transition in this weak coupling theory.

We have reported exact diagonalisation calculations for Hamiltonian (2) of finite lattices.^{23,24} These studies suggested that, for parameters relevant to $\text{Na}_{0.5}\text{CoO}_2$, the system is a covalent insulator, with little charge disproportionation and a small gap $\sim |t|$, rather than a charge ordered insulator, with strong charge disproportionation and a gap $\sim \Delta$. This prediction is consistent with the experimental measurements of the

charge disproportionation.^{26,27,41} Further, these calculations predict a gap of the same order of magnitude as in seen in the ARPES⁶ and the resistivity,⁴ predict the large moment seen in neutron scattering,^{31,37} and reproduce the main features seen in the optical conductivity.⁵ Zhou and Wang⁴⁵ also studied a model that incorporates the effects of Na-ordering within the Gutzwiller approximation and found it could explain many of the experimental observations.

There has been significantly less work on $\text{K}_{0.5}\text{CoO}_2$ and $\text{Rb}_{0.5}\text{CoO}_2$. Lee and Pickett⁴⁶ have reported LDA calculations for $\text{K}_{0.5}\text{CoO}_2$ and compared these with equivalent calculations for $\text{Na}_{0.5}\text{CoO}_2$. They found that the t_{2g} band is rather narrower in $\text{K}_{0.5}\text{CoO}_2$ than $\text{Na}_{0.5}\text{CoO}_2$ and that the Fermi surface is more complicated in $\text{K}_{0.5}\text{CoO}_2$ as there are several small pockets along the X - S line. They speculated that these pockets, some of which are quite well nested near the X point, may lead to enhanced magnetic tendencies in $\text{K}_{0.5}\text{CoO}_2$.

Clearly an important question is: what parameters in Hamiltonian (2) correspond to the various possible choices of A in $A_{0.5}\text{CoO}_2$? Various atomistic calculations that address this question have been presented for $A=\text{Na}$, but for other A there are not yet suitable estimates. CAS+DDCI calculations⁴⁷ on small clusters of $\text{Na}_{0.5}\text{CoO}_2$ give $-t = 0.08 - 0.14$ eV, $U = 2.5 - 2.8$ eV, and $\Delta = 0.16$ eV. For bulk $\text{Na}_{0.5}\text{CoO}_2$ the LDA yields $\Delta = 0.07$ eV⁹ and $t \simeq -0.1$ eV^{43,48}, and electrostatic Ewald calculations give¹⁰ $\Delta = 0.03 - 0.05$ eV. Furthermore, CoO_2 , which is described by Hamiltonian (2) at half filling with $\Delta = 0$, is observed to be a strongly correlated metal rather than a Mott insulator.⁴⁹ This suggests that $U \lesssim U_c \sim 12 - 15t$, where U_c is the critical value for formation of a Mott insulator on the triangular lattice.^{2,50} Hence, realistic parameters for $\text{Na}_{0.5}\text{CoO}_2$ may be in the range $10 < U/|t| < 15$, and $0.5 < |\Delta/t| < 2$.

The negative sign of t is natural if the hopping between Co sites is dominated by the contribution from hopping via an intermediate O site. To leading order this gives $t = -|t_{\text{CoO}}|^2/(\epsilon_{\text{Co}} - \epsilon_{\text{O}})$, where t_{CoO} is the direct hopping between a Co atom and a neighbouring O atom, ϵ_{Co} is the energy of an electron in a d orbital centred on a Co atom, and ϵ_{O} is the energy of an electron in a p orbital centred on an O atom (note that one expects that $\epsilon_{\text{Co}} > \epsilon_{\text{O}}$).

II. SLAVE BOSON THEORY OF STRONGLY-INTERACTING ELECTRONS

We now investigate paramagnetic phases of the $U \rightarrow \infty$ limit of the ionic Hubbard model by deriving a mean field theory using Barnes-Coleman slave bosons.⁵¹ The $U \rightarrow \infty$ limit greatly simplifies the analysis and is not unreasonable in spite of our estimate, above, that $10 < U/|t| < 15$. Our previous exact diagonalization calculations^{23,24} show that, provided $U \gg |t|$ the physics

of this model is insensitive to particular value of $U/|t|$. Specifically, our results for $U = 10|t|$ show only minor quantitative differences from those for $U = 100|t|$.

A. Theory of the metallic state

We begin by making the particle-hole transformation $\hat{c}_{i\alpha\sigma} \rightarrow \hat{h}_{i\alpha\sigma}^\dagger$. We then introduce the slave bosons. Following, for example, Ref. 52, we write

$$\hat{h}_{i\alpha\sigma}^\dagger = \hat{f}_{i\alpha\sigma}^\dagger \hat{b}_{i\alpha} + \sum_{\sigma'} \epsilon_{\sigma\sigma'} \hat{f}_{i\alpha\sigma'} \hat{d}_{i\alpha}^\dagger, \quad (3)$$

where $\epsilon_{\sigma\sigma'}$ is the completely antisymmetric tensor, $\hat{f}_{i\alpha\sigma}^{(\dagger)}$ annihilates (creates) a fermion with spin σ at site i on sublattice α , $\hat{d}_{i\alpha}^{(\dagger)}$ annihilates (creates) a boson, corresponding to a site that is doubly occupied by holes, at site i on sublattice α , and $\hat{b}_{i\alpha}^{(\dagger)}$ annihilates (creates) a boson, corresponding to a site containing no holes, at site

i on sublattice α . If the number of holes is less than or equal to the number of lattice sites and $U = \infty$ there is zero weight for configurations containing any sites doubly occupied (with holes) in the the ground state or any excited states at finite energy above the ground state. Therefore, $\hat{d}_{i\alpha}$ can be ‘deleted’ giving us

$$\hat{h}_{i\alpha\sigma}^\dagger = \hat{f}_{i\alpha\sigma}^\dagger \hat{b}_{i\alpha}. \quad (4)$$

It is clear from Eq. (4) that the \hat{f} ’s are hole-like operators. This transformation is exact, in the limit $U \rightarrow \infty$, provided we impose the constraint

$$1 = \sum_{\sigma} \hat{f}_{i\mu\sigma}^\dagger \hat{f}_{i\mu\sigma} + \hat{b}_{i\mu}^\dagger \hat{b}_{i\mu} \equiv \hat{Q}_{i\mu} \quad (5)$$

on the system.

Hence, we find that the Hamiltonian (2) may be written as

$$\hat{\mathcal{H}} - \mu \hat{N} = t \sum_{\langle ij\alpha\beta \rangle \sigma} \hat{f}_{i\alpha\sigma}^\dagger \hat{f}_{j\beta\sigma} \hat{b}_{j\beta}^\dagger \hat{b}_{i\alpha} + \frac{\Delta}{2} \sum_i \left(\hat{b}_{iA}^\dagger \hat{b}_{iA} - \hat{b}_{iB}^\dagger \hat{b}_{iB} \right) - \mu \sum_{i\beta} (1 + \hat{b}_{i\beta}^\dagger \hat{b}_{i\beta}) \quad (6)$$

We make a mean-field approximation by replacing the bosons by the expectation value $q_{ij\alpha\beta} \equiv \langle \hat{b}_{i\alpha}^\dagger \hat{b}_{j\beta} \rangle$, which gives,

$$\hat{\mathcal{H}}_{\text{mf}} - \mu \hat{N} = t \sum_{\langle ij\alpha\beta \rangle \sigma} \hat{f}_{i\alpha\sigma}^\dagger \hat{f}_{j\beta\sigma} q_{ji\beta\alpha} + \frac{\Delta}{2} \sum_i (q_{iiAA} - q_{iiBB}) - \mu \sum_{i\beta} (1 + q_{ii\beta\beta}) \quad (7)$$

We now assume that the bosonic mean field is homogeneous ($q_{ij\alpha\beta} = q_{\alpha\beta}$) and introduce the Lagrange multipliers, λ_α to enforce, on average, the local constraints [via the term $-\sum_{i\alpha} \lambda_\alpha (1 - Q_{i\alpha})$]. Thus one finds that

$$\hat{F} \equiv \hat{\mathcal{H}}_{\text{mf}} - \mu \hat{N} - \sum_{i\alpha} \lambda_\alpha (1 - \hat{Q}_{i\alpha}) \quad (8)$$

$$= t \sum_{\langle ij\alpha\beta \rangle \sigma} \hat{f}_{i\alpha\sigma}^\dagger \hat{f}_{j\beta\sigma} q_{\beta\alpha} + \frac{\Delta}{2} \sum_i (q_{AA} - q_{BB}) - \mu \sum_{i\beta} (1 + q_{\beta\beta}) - \sum_{i\beta} \lambda_\beta \left(1 - q_{\beta\beta} - \sum_{\sigma} \hat{f}_{i\beta\sigma}^\dagger \hat{f}_{i\beta\sigma} \right).$$

Upon performing a Fourier transform one finds that there are two bands, which we denote the bonding (-) and antibonding (+) bands,

$$\begin{aligned} \hat{F} &= \sum_{\mathbf{k}\sigma} \begin{pmatrix} \hat{f}_{\mathbf{k}A\sigma} \\ \hat{f}_{\mathbf{k}B\sigma} \end{pmatrix}^\dagger \begin{pmatrix} 2tq_{AA} \cos k_x + \lambda_A & 4tq_{AB} \cos \frac{k_x}{2} \cos \frac{k_y}{2} \\ 4tq_{BA} \cos \frac{k_x}{2} \cos \frac{k_y}{2} & 2tq_{BB} \cos k_x + \lambda_B \end{pmatrix} \begin{pmatrix} \hat{f}_{\mathbf{k}A\sigma} \\ \hat{f}_{\mathbf{k}B\sigma} \end{pmatrix} \\ &\quad + N \left\{ \frac{\Delta}{2} (q_{AA} - q_{BB}) - \sum_{\nu} [\mu(1 + q_{\nu\nu}) + \lambda_{\nu}(1 - q_{\nu\nu})] \right\} \end{aligned} \quad (9)$$

$$\begin{aligned} &\equiv \sum_{\mathbf{k}\sigma} \begin{pmatrix} \hat{\psi}_{\mathbf{k}+\sigma} \\ \hat{\psi}_{\mathbf{k}-\sigma} \end{pmatrix}^\dagger \begin{pmatrix} E_{\mathbf{k}+\sigma} & 0 \\ 0 & E_{\mathbf{k}-\sigma} \end{pmatrix} \begin{pmatrix} \hat{\psi}_{\mathbf{k}+\sigma} \\ \hat{\psi}_{\mathbf{k}-\sigma} \end{pmatrix} \\ &\quad + N \left\{ \frac{\Delta}{2} (q_{AA} - q_{BB}) - \sum_{\nu} [\mu(1 + q_{\nu\nu}) + \lambda_{\nu}(1 - q_{\nu\nu})] \right\} \end{aligned} \quad (10)$$

TABLE I: Physical meaning of the mean fields, q_i , and the Lagrange multipliers, λ_{\pm} . Note that one can also interpret the quasiparticle weights as the inverse of the corresponding effective mass.

Parameter	Alternative symbol	meaning
q_+	Z_+	uniform intra-chain quasiparticle weight
q_-	Z_-	anisotropic intra-chain quasiparticle weight
$ q_{AB} $	Z_{AB}	inter-chain quasiparticle weight
q_{AA}	Z_{AA}	A-sublattice intra-chain quasiparticle weight
q_{BB}	Z_{BB}	B-sublattice intra-chain quasiparticle weight
$-\lambda_+$	μ^*	effective quasihole chemical potential
$-\lambda_-$	$\Delta^*/2$	effective ionic potential

where k_x and k_y are defined in the reduced $(1 \times \sqrt{3})$ Brillouin zone of the model (Fig. 1e), $N = \sum_i$ is the number of unit cells, i.e., half the number of lattice sites, and the dispersion relations, $E_{\mathbf{k}\pm\sigma}$, of the ‘quasiholes’, which are destroyed (created) by $\hat{\psi}_{\mathbf{k}\pm\sigma}^{(\dagger)}$, are given by

$$E_{\mathbf{k}\pm\sigma} = 2tq_+ \cos k_x + \lambda_+ \pm \sqrt{[2tq_- \cos k_x + \lambda_-]^2 + 16t^2|q_{AB}|^2 \cos^2 \frac{k_x}{2} \cos^2 \frac{k_y}{2}} \quad (11)$$

where $q_+ = \frac{1}{2}(q_{AA} + q_{BB})$, $q_- = \frac{1}{2}(q_{AA} - q_{BB})$, $\lambda_+ = \frac{1}{2}(\lambda_A + \lambda_B)$, and $\lambda_- = \frac{1}{2}(\lambda_A - \lambda_B)$.

Hence we find that

$$\begin{aligned} \hat{F} = \sum_{\mathbf{k}\alpha\sigma} & \left\{ 2tq_+ \cos k_x + \lambda_+ + \alpha \sqrt{[2tq_- \cos k_x + \lambda_-]^2 + 16t^2|q_{AB}|^2 \cos^2 \frac{k_x}{2} \cos^2 \frac{k_y}{2}} \right\} \hat{\psi}_{\mathbf{k}\alpha\sigma}^\dagger \hat{\psi}_{\mathbf{k}\alpha\sigma} \\ & + 2N \left[\left(\frac{\Delta}{2} + \lambda_- \right) q_- - \mu(1 + q_+) - \lambda_+(1 - q_+) \right], \end{aligned} \quad (12)$$

where $\alpha \in \{\pm 1\}$.

It is interesting to compare this with the solution of the model with $U = 0$ [see Appendix A and particularly Eq. (A1)]. This enables a straightforward identification of the physical meaning of the mean fields q_{\pm} and q_{AB} and the Lagrange multipliers λ_{\pm} , see table I.

It follows from the the approximation that the bosonic mean-field is homogeneous and the constraint of one particle per site that, at three-quarters filling, we need only consider a two site model (i.e., one unit cell), which must contain exactly one boson. Thus, the bosonic wavefunction may be written as

$$|\Psi\rangle = \prod_i \left(v e^{i\theta} \hat{b}_{iA}^\dagger + \sqrt{1 - v^2} \hat{b}_{iB}^\dagger \right) |0\rangle, \quad (13)$$

where v is a real number between 0 and 1. Thus

$$q_{AA} = \langle \Psi | \hat{b}_{iA}^\dagger \hat{b}_{iA} | \Psi \rangle = v^2 \quad (14a)$$

$$q_{BB} = \langle \Psi | \hat{b}_{iB}^\dagger \hat{b}_{iB} | \Psi \rangle = 1 - v^2 \quad (14b)$$

$$q_{AB} = \langle \Psi | \hat{b}_{iA}^\dagger \hat{b}_{iB} | \Psi \rangle = v(1 - v)e^{-i\theta} = \sqrt{q_{AA}q_{BB}}e^{-i\theta} = \sqrt{q_+^2 - q_-^2}e^{-i\theta}. \quad (14c)$$

Therefore, the total energy of the model is

$$\begin{aligned} F \equiv \langle \hat{F} \rangle = \sum_{\mathbf{k}\alpha\sigma} & \left\{ 2tq_+ \cos k_x + \lambda_+ + \alpha \sqrt{[2tq_- \cos k_x + \lambda_-]^2 + 16t^2(q_+^2 - q_-^2) \cos^2 \frac{k_x}{2} \cos^2 \frac{k_y}{2}} \right\} n_{\mathbf{k}\alpha\sigma} \\ & + 2N \left[\left(\frac{\Delta}{2} + \lambda_- \right) q_- - \mu(1 + q_+) - \lambda_+(1 - q_+) \right], \end{aligned} \quad (15)$$

where $n_{\mathbf{k}\alpha\sigma} \equiv \langle \hat{\psi}_{\mathbf{k}\alpha\sigma}^\dagger \hat{\psi}_{\mathbf{k}\alpha\sigma} \rangle$. The phase θ does not change the energy, thus, the solution has a U(1) degeneracy above that found in the slave boson mean field theory of the Hubbard model⁵² due to the two sublattice structure of the problem.

It is straightforward to show that $q_+ = x = 1/2$ follows from the requirement that $-\partial F/\partial\mu = N_e$, where the total number of electrons is $N_e = \sum_{i\mu\sigma} \hat{c}_{i\mu\sigma}^\dagger \hat{c}_{i\mu\sigma} = 2N(1+x)$ for $A_x\text{CoO}_2$ and we have specialised to $x = 1/2$, which is the relevant filling. This result fits with our intuition that, on average, there should be one boson (i.e., one doubly occupied site) per unit cell.

Similarly, $(2N)^{-1} \sum_{\mathbf{k}\alpha\sigma} n_{\mathbf{k}\alpha\sigma} = (1 - q_+) = \frac{1}{2}$ follows from the requirement that F is an extremum with respect to λ_+ . Again, this fits with our intuition that there is, on average, one quasihole fermion (singly occupied site) per unit cell.

Three more complicated intertwined self-consistency conditions can also be derived:

$$\lambda_- = -\frac{\Delta}{2} - \frac{1}{2N} \sum_{\mathbf{k}\alpha\sigma} \alpha \left\{ \frac{[2tq_- \cos k_x + \lambda_-] 2t \cos k_x - 16t^2 q_- \cos^2 \frac{k_x}{2} \cos^2 \frac{k_y}{2}}{\sqrt{[2tq_- \cos k_x + \lambda_-]^2 + 16t^2 (q_+^2 - q_-^2) \cos^2 \frac{k_x}{2} \cos^2 \frac{k_y}{2}}} \right\} n_{\mathbf{k}\alpha\sigma} \quad (16a)$$

follows from the requirement that F is a minimum with respect to q_- ;

$$q_- = -\frac{1}{2N} \sum_{\mathbf{k}\alpha\sigma} \alpha \left\{ \frac{2tq_- \cos k_x + \lambda_-}{\sqrt{[2tq_- \cos k_x + \lambda_-]^2 + 16t^2 (q_+^2 - q_-^2) \cos^2 \frac{k_x}{2} \cos^2 \frac{k_y}{2}}} \right\} n_{\mathbf{k}\alpha\sigma} \quad (16b)$$

follows from the requirement that F is an extremum with respect to λ_- ; and

$$\mu = \sum_{\mathbf{k}\alpha\sigma} \left\{ 2t \cos k_x + \alpha \frac{16t^2 q_+ \cos^2 \frac{k_x}{2} \cos^2 \frac{k_y}{2}}{\sqrt{[2tq_- \cos k_x + \lambda_-]^2 + 16t^2 (q_+^2 - q_-^2) \cos^2 \frac{k_x}{2} \cos^2 \frac{k_y}{2}}} \right\} n_{\mathbf{k}\alpha\sigma} + \lambda_+ \quad (16c)$$

follows from the requirement that F is a minimum with respect to q_+ .

In order to compare our results with ARPES experiments on $\text{Na}_{0.5}\text{CoO}_2$ and $\text{K}_{0.5}\text{CoO}_2$ we calculate the spectral function, $A(\mathbf{k}, \omega) \equiv \frac{1}{\pi} \text{Im} \text{Tr} G_{\mu\nu\sigma\sigma'}(\mathbf{k}, \omega)$, where $G_{\mu\nu\sigma\sigma'}(\mathbf{k}, \omega)$ is the electronic propagator. In real space and time the one electron propagator is given by

$$\begin{aligned} iG_{ij\mu\nu\sigma\sigma'}(t) &\equiv \langle \hat{c}_{i\mu\sigma}^\dagger(t) c_{j\nu\sigma'}(0) \rangle \\ &= q_{\mu\nu} \langle \hat{f}_{i\mu\sigma}(t) f_{j\nu\sigma'}^\dagger(0) \rangle \end{aligned} \quad (17)$$

Fourier transforming and taking the trace, one finds that

$$A(\mathbf{k}, \omega) = 2 \sum_{\alpha} Z_{\mathbf{k}\alpha} [1 - n_F(E_{\mathbf{k}\alpha\sigma})] \delta(E_{\mathbf{k}\alpha\sigma} - \omega), \quad (18)$$

where n_F is the Fermi function,

$$Z_{\mathbf{k}\alpha} = q_+ + \alpha \cos 2\theta_{\mathbf{k}} \quad (19)$$

is the quasiparticle weight, and

$$\tan \theta_{\mathbf{k}} = \frac{E_{\mathbf{k}+\uparrow} - 2t(q_+ + q_-) \cos k_x + \lambda_+ + \lambda_-}{4t\sqrt{q_+^2 - q_-^2} \cos \frac{k_x}{2} \cos \frac{k_y}{2}}. \quad (20)$$

Therefore, we find that, in contrast to mean field slave boson theories of other models, the quasiparticle weight is momentum dependent in the theory of the ionic Hubbard model. However, this does not mean that all non-local correlations induced by the on-site Coulomb repulsion are included in the present approach.

B. Theory of the insulating state

With any minimisation over a finite parameter space it is important to check explicitly whether any of the end points are the global minima.⁵³ Therefore we must consider the special case $q_- = \pm 1/2$ separately from the general set of self consistency conditions [Eqs. (16)]. Let us consider the case of large (how large will be determined later) positive Δ such that $q_- = -1/2$, recall that $q_+ = 1/2$. Eq. (9) then yields

$$\begin{aligned} F &= \sum_{\mathbf{k}\sigma} [(2t \cos k_x + \lambda_B) n_{\mathbf{k}B\sigma} + \lambda_A n_{\mathbf{k}A\sigma}] \\ &\quad - N \left(\frac{\Delta}{2} + 3\mu + \lambda_A \right). \end{aligned} \quad (21)$$

Therefore $-\partial F/\partial\mu = 3N$, as is required to ensure three electrons per unit cell. Further, one finds that $n_{\mathbf{k}B\sigma} = 0$ for all \mathbf{k} and σ from the requirement that F is an extremum with respect to λ_B , which we expect from $q_B = 1$ and the constraint of one particle per cite. Finally, $\sum_{\mathbf{k}\sigma} n_{\mathbf{k}A\sigma} = N$ due to the requirement that F is an extremum with respect to λ_A , which is simply the expected constraint that the A sublattice is half filled with quasiholes. Note, however, that because of the infinite U or, equivalently, the constraint of one particle per site, the half filled A sublattice is insulating. This is also reflected in the fact that $q_{AA} = q_{AB} = 0$, i.e. there is zero quasiparticle weight for fermions on the A sublattice. So

the state $q_A = 0$, $q_B = 1$ (or, equivalently, $q_+ = 1/2$, $q_- = -1/2$) describes a charge transfer insulator, which has the characteristics of both Mott (A sublattice) and band (B sublattice) insulators. Thus, we find that,

$$\frac{F}{N} = -\frac{\Delta}{2} - 3\mu, \quad (22)$$

which is clearly just the classical energy of paramagnetic insulating state.

C. Comparison with the empirical theory of Choy *et al.*

As discussed in section I B, Choy *et al.*⁴² have studied an empirical model Hamiltonian for holes and doublons motivated by the presumed low energy processes about an antiferromagnetically ordered charge transfer insulating state. This empirical model gives good agreement with the measured temperature dependence of both the resistivity and the Hall coefficient. It is therefore interesting to compare our Eq. (9) with the Hamiltonian studied by Choy *et al.* [their Eq. (2)].

Upon making the following notational changes to and substitutions into Eq. (9): $t_{qAA} \rightarrow -t_{ij}^d$; $t_{qBB} \rightarrow t_{ij}^h$; $\lambda_- \rightarrow V + \tilde{J}$; $t_{qAB} \rightarrow t$; $\hat{f}_{iB\sigma} \rightarrow h_{i\sigma}$; $\sum_{\sigma} \hat{f}_{iA\sigma}^{\dagger} \hat{f}_{jA\sigma} = \delta_{ij} - \hat{b}_{iA}^{\dagger} \hat{b}_{jA}$; $\hat{b}_{iA} \rightarrow d_i$; $\hat{b}_{iA}^{\dagger} \hat{f}_{jB\sigma} = \hat{f}_{iA\sigma} \hat{f}_{jB\sigma}$ and neglecting constant terms one finds that the two Hamiltonians are identical. Notice, in particular, that the renormalised ionic potential, λ_- , in our theory plays the role of the inter-site interactions, $V + \tilde{J}$, in that of Choy *et al.* Also their non-magnetic regime ($\alpha = 0$) corresponds to $q_- = 0$ in our slave boson theory. The ground state studied by Choy *et al.* corresponds to the charge transfer insulator we only find for $|\Delta/t| \gg 1$. Thus, at least in this regime, the two theories appear to be equivalent. In order to get agreement with the experimentally measured temperature dependence of the resistivity and the Hall coefficient Choy *et al.* require a specific temperature dependence of (in our notation) q_{AA} , q_{BB} , and λ_- . Although we will not present finite temperature calculations below, such a temperature dependence is a quite reasonable expectation for our mean field theory. Indeed slave boson mean-field theories of other strongly correlated models have boson mean-fields, similar to $q_-(T)$, that decrease monotonically with increasing temperature and vanish at some coherence temperature, $T^* \ll T_F^0$, the Fermi temperature of the non-interacting system.^{54,55}

III. NUMERICAL RESULTS

We have solved the self consistent equations (16) on an $L \times L$ reciprocal space mesh for $L = 100$ and 1000. For the $L = 1000$ solutions we also tightened the convergence criteria by a factor of 50. We find that the solutions are well converged as the difference between the $L = 100$ and

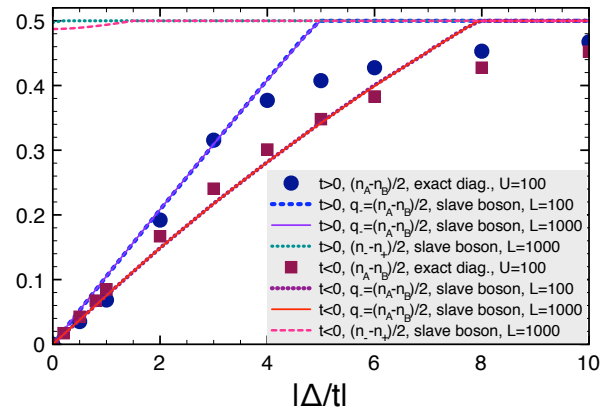


FIG. 2: [Color online] Charge disproportionation as a function of $|\Delta/t|$ for both signs of t . Here we compare the real-space charge disproportionation, $n_A - n_B$, calculated by exact diagonalisation²³ with the results from the slave boson calculations where $q_- = (n_A - n_B)/2$. The two methods are in excellent quantitative agreement for small $|\Delta/t|$, but at large $|\Delta/t|$ the slave boson theory predicts complete charge disproportionation, i.e., one sublattice becomes completely filled. In the exact diagonalisation results complete charge disproportionation is only approached asymptotically as $|\Delta/t| \rightarrow \infty$. In the slave boson theory the system is metallic except when there is complete charge disproportionation. In the exact diagonalisation calculations a gap opens when there is only a small charge transfer between the two sublattices. We also plot the reciprocal space (band) charge disproportionation, $n_- - n_+$. We see that the MIT does not occur at the same $|\Delta/t|$ as the bonding band becomes filled, in spite of this implying that the antibonding band is half filled and the fact that $U = \infty$. This emphasises the fact that the half filled band is *not* equivalent to a half filled 1D chain. We plot q_- (similar results are found for other parameters) for two different sized ($L \times L$) reciprocal space meshes. In the $L = 1000$ case the convergence criteria is also tightened by a factor of 50, which demonstrates that the calculations are well converged.

$L = 1000$ self consistent solutions is no larger than a few parts in a thousand for any of the parameters. By way of an example, in Fig. 2 we report both sets of results, it can be seen the difference in the results is significantly smaller than the width of the lines. Therefore, we report only the $L = 1000$ results in the subsequent figures.

A. Charge disproportionation and the metal-charge ordered insulator transition

In Fig. 2 we plot the real space charge disproportionation, $q_- = (n_A - n_B)/2$, where $n_{\mu} = \langle \sum_{i\sigma} \hat{c}_{i\mu\sigma}^{\dagger} \hat{c}_{i\mu\sigma} \rangle$ is the average number of *electrons* per sublattice site, against $|\Delta/t|$. It can be seen that the results are strongly dependent on the sign of t . The system is metallic for $|q_-| < 1/2$; $|q_-| = 1/2$ corresponds to exactly one fermion on each site of the A-sublattice and exactly one boson on each site of the B-sublattice. The metal-insulator transition (MIT) occurs at $|\Delta/t| = 8.0$ for $t < 0$

and $|\Delta/t| = 5.0$ for $t > 0$.

We also plot the reciprocal space charge disproportionation (band filling) in Fig. 2. For $t > 0$ the bonding band is filled for all non-zero Δ/t (for $\Delta = 0$ the unit cell is halved so there is only a single band). For $t < 0$ the bonding band is only partially filled for $|\Delta/t| < 1.5$. As we will discuss in detail below, the quasiparticles in the bonding (-) band are significantly lighter than those in the, nearly half-filled, antibonding (+) band. It is interesting to observe therefore that for $t < 0$, $1.5 < |\Delta/t| < 8.0$ and $t > 0$, $0 < |\Delta/t| < 5.0$ the antibonding band is half-filled and, even though $U = \infty$, the system remains metallic. At first sight this is rather surprising as the system is two-dimensional and even quasi-one-dimensional. However, because the bands arise from the hybridisation of the A and the B sublattices the usual real space arguments that explain the Mott insulating state do not apply here. There is no interaction between the quasiparticles other than the real space constraint of one fermion (or boson) per site. Therefore, unless there is complete charge disproportionation the system remains metallic.

It is interesting to contrast the results of the slave boson calculations with our previous exact diagonalisation results for finite clusters with $U = 100|t|$.^{23,24} At least at low $|\Delta/t|$, the slave boson theory gives excellent agreement with the exact diagonalisation for some physical quantities, e.g., the level of charge disproportionation (cf. Fig. 2). But, there is an important qualitative difference between the slave boson calculations and the exact diagonalisation results: the nature of the insulating state. In the slave boson calculations an insulating state is only realised when there is complete charge disproportionation leaving one sublattice completely filled and the other half-filled. The filled sublattice acts as a band insulator and, because $U = \infty$, the half filled sublattice becomes a Mott insulator. This charge transfer insulator is very different from the covalent insulating state predicted from the exact diagonalisation calculations.^{23,24} These calculations predict that the insulating state occurs at quite small values of $|\Delta/t|$ in spite of there being only rather weak charge disproportionation. This insulating state depends crucially on the hybridisation between the two sublattices and is analogous to a covalent insulator.⁵⁶ Our mean field theory neglects non-local correlations that are included in the exact diagonalisation calculations and cause the covalent insulating state. Preliminary results suggest that DMFT, which also neglects non-local correlations but is more sophisticated than our mean field theory, cannot describe the covalent insulator phase either.

In Figs. 3 and 4 we plot the ground state energy, F , as a function of q_- for various values of $|\Delta/t|$ and the self consistently calculated curve of F against q_- with $|\Delta/t|$ as a parametric parameter. It can be seen from these plots that the self consistent solutions are the true minima. Further, the absence of double well structures in the plots of F against q_- strongly suggest that the MIT is a second order phase transition in the slave boson theory.

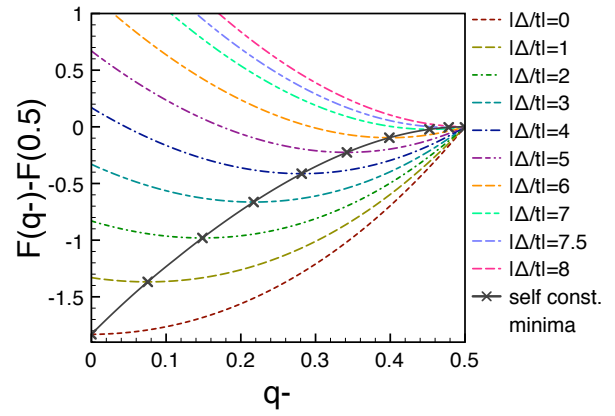


FIG. 3: [Color online] The ground state energy, F , relative to that in the insulating state for the same value of Δ as a function of q_- for various values of Δ and $t < 0$. The solid black line indicates the free energy found at the self consistent solution, with crosses marking the data for values of Δ at which we plot the full $F(q_-)$ curve. This plot indicates that the self consistent solutions are indeed minima of F with respect to the variation of q_- [note that Eq. (16a) only requires that the self consistent solution is a turning point in F with respect to q_- , whereas, physically, we seek the minimum]. These results also strongly suggest that the metal insulator transition in the slave boson theory is second order as no double well structure is seen in $F(q_-)$.

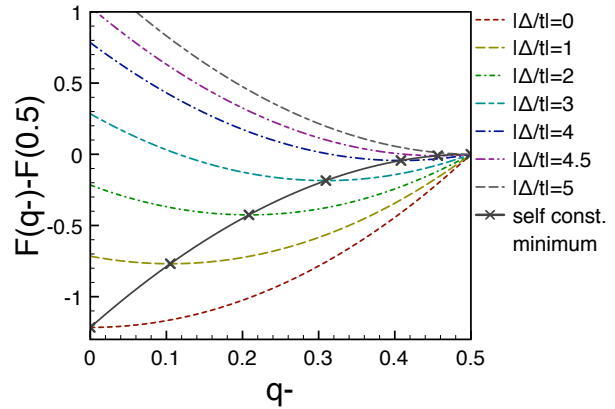


FIG. 4: [Color online] Same as Fig. 3 but for $t > 0$. Again this shows that the self consistent solutions are true minima, and that the metal-charge ordered insulator transition is second order.

B. Band structure of the fermionic quasiholes

We now turn to analyse the properties of the fermionic quasiholes. As these are non-interacting particles one can straightforwardly calculate the properties of the quasiholes. It is interesting to compare these results with the band structure of the non-interacting ($U = 0$) ionic Hubbard model, which we discuss in Appendix A.

Before discussing the band structure in detail we should point out that the bands are, to some extent, an

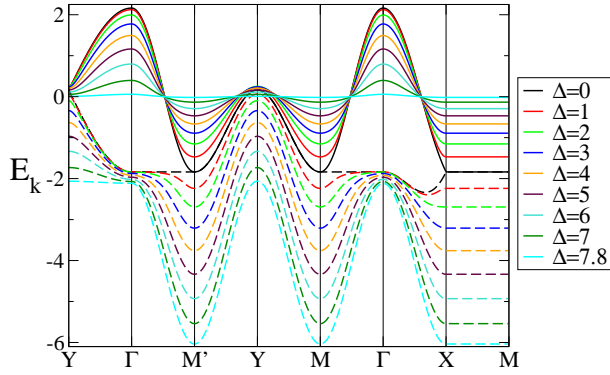


FIG. 5: [Color online] Band structure of the fermions for $t < 0$. The band structure is not unlike that of the non-interacting system (Fig. 14). However, for the fermions, increasing $|\Delta/t|$ has a much stronger effect than it does for the non-interacting electrons. In particular as $|\Delta/t|$ is increased the antibonding band (solid lines) is flattened and eventually becomes flat when the metal-insulator transition is reached at $|\Delta/t| = 8.0$. The high symmetry points of the first Brillouin zone

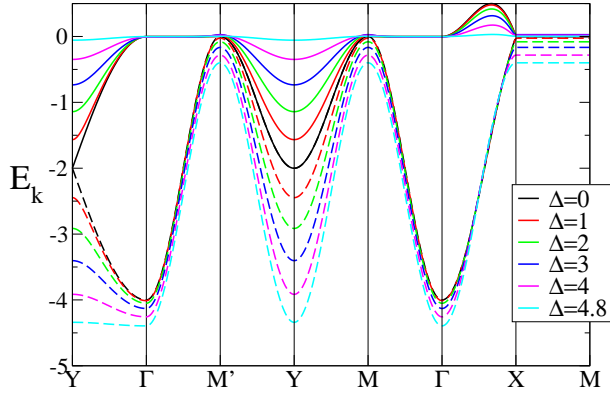


FIG. 6: [Color online] Band structure of the fermions for $t > 0$. There are significant differences from the band structure of $t < 0$ (Fig. 5). In particular the metal-insulator transition occurs at only $|\Delta/t| = 5.0$. Also see the online movie.⁵⁷

artefact of the mean field approximation. In the exact solution correlations that are not captured by the mean field approximation may destroy the description of the system in terms of extended bands (cf. Ref. 24). Nevertheless, if the mean field theory does provide a reasonable description of the ionic Hubbard model then one expects that some of the features of the band structure described below do survive in the exact solution. Further, the bands are well defined in the mean-field slave-boson theory. Therefore, it is legitimate to calculate their properties in this context and this is extremely useful for building intuition about this problem.

Figs. 5 and 6 show how the dispersion relations of the fermionic quasiholes vary with $|\Delta/t|$ for each sign of t (also see the animations online⁵⁷). These should be compared with the equivalent plots (Figs. 14 and 15) for the

non-interacting system. It can be seen that at $\Delta = 0$, for both signs of t , the quasiparticle bands are significantly narrower than the equivalent non-interacting electron bands. As $|\Delta/t|$ increases the antibonding band narrows and eventually becomes flat at the MIT. While the bonding band broadens somewhat as $|\Delta/t|$ increases.

These conclusions are consistent with changes observed in the density of states, which we plot in Figs. 7 and 8 (also see the animations online⁵⁷), calculated by treating the fermions as non-interacting particles. These figures should be contrasted with the equivalent plots of the non-interacting system (Figs. 18 and 19). For both signs of t as $|\Delta/t|$ is increased the antibonding band narrows into the quasiparticle peak, familiar from the Mott-Hubbard transition.⁵⁸ Note that, as the fermions are hole-like, the states with $E > 0$ are filled and the states with $E < 0$ are unoccupied.

We plot the the Fermi surfaces of the quasiholes in Figs. 9 and 10. Both signs of t exhibit strong nesting, suggesting that there may be magnetic instabilities, which we do not consider here. For $t < 0$ and $|\Delta/t| < 1.5$ there are small two-dimensional Fermi pockets of light quasiholes arising from the bonding band, as well as the quasi-one-dimensional sheets arising from the antibonding band. For $|\Delta/t| \rightarrow 0$ the small Fermi pocket occupies 0.7% of the Brillouin zone. As $|\Delta/t|$ increases the Fermi pocket shrinks and it vanishes at $|\Delta/t| = 1.5$.

In the $A_{0.5}\text{CoO}_2$ materials the unit cells are twice the size of that of our model. This results in a zone folding of the Brillouin zone in the x -direction, cf. Fig. 1. This will result in the formation of additional small pockets around the X and M points (of the $A_{0.5}\text{CoO}_2$ Brillouin zone, Fig. 1f), which are formed from fermions in the antibonding band. If one simply folds our results into the $A_{0.5}\text{CoO}_2$ Brillouin zone the pockets from the bonding band occupy 1.4% of the Brillouin zone for $|\Delta/t| \rightarrow 0$ (as the Brillouin zone has halved in size, while the pocket area remains unchanged) and the pockets around the X and M points arising from the antibonding band occupy 8.6% and 9.9% of the Brillouin zone respectively.

C. Spectral density

The combination of small $|\Delta/t|$ and large $U/|t|$ significantly changes the dispersion relations of the quasiparticles from those of the non-interacting electrons, compare section IIIB with Appendix A and particularly Figs. 5 and 6 with Figs. 14 and 15. First, the antibonding band has a much weaker dispersion than for $U = 0$ than for $U = \infty$. This is seen in ARPES experiments on $\text{Na}_{0.5}\text{CoO}_2$ and $\text{K}_{0.5}\text{CoO}_2$, where the measured Fermi velocity is several times smaller than the value calculated from the LDA with no sodium ion ordering (cf. Fig. 2i of Ref. 6). As Δ increases weight gets shifted from the antibonding to the bonding band.

We plot two different reciprocal space cuts of the calculated spectral function for representative values of

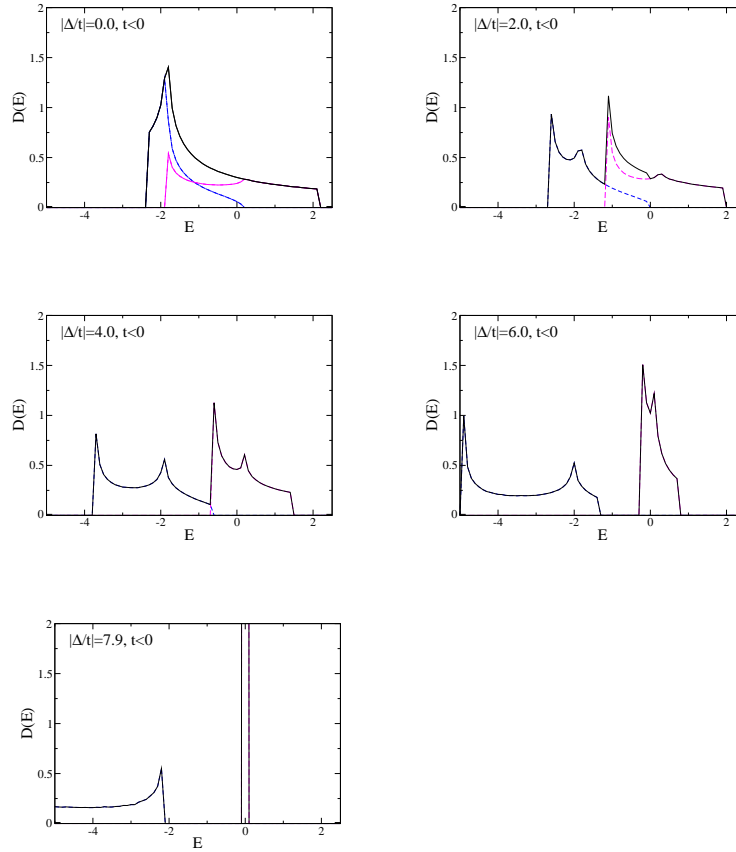


FIG. 7: [Color online] Density of states (in units where $|t| = a = 1$) of the fermions for $t < 0$. Dashed (blue and pink) lines indicate the contributions of the individual bands. The narrowing of the antibonding band, as $|\Delta/t|$ increases, is clearly visible from these plots, while it can be seen that the bonding band actually becomes a little wider as $|\Delta/t|$ increases. Clearly, the DOS is very different from the non-interacting case, cf. Fig. 18, and these difference become greater as $|\Delta/t|$ increases. Also see the online movie.⁵⁷

$|\Delta/t|$ and $t < 0$ in Figs. 11 and 12 (also see the animations online⁵⁷). As shown in Fig. 1, the unit cells of $A_{0.5}\text{CoO}_2$ are twice as large as the unit cell of Hamiltonian (2). In order to facilitate comparison with experiment, we have plotted these results in the Brillouin zone of $\text{Na}_{0.5}\text{CoO}_2$ by ‘folding over’ the results for Hamiltonian (2) into the Brillouin zone of the actual materials. At $T = 0$ Eq. (18) gives a plane of δ -functions (in the three dimensional \mathbf{k}, ω space). It is well known that

$$\delta(\epsilon - \omega) = \lim_{b \rightarrow 0} \frac{\exp[-(\epsilon - \omega)^2/4b]}{2\sqrt{\pi b}}. \quad (23)$$

Therefore we have broadened the results by replacing the δ -function with a Gaussian with $b = 0.01t^2$. We report our results with the Fermi factor appropriate for $k_B T = |t|/60 \simeq 20$ K for $-t = 0.1$ eV.

It can be seen from Figs. 11 and 12 that as $|\Delta/t|$ is increased the antibonding band remains at the Fermi energy, but loses spectral weight, consistent with the calculated density of states for fermions (Figs. 7 and 8). Meanwhile, the bonding band is shifted down in energy. In the Γ -M cut (Fig. 11) we see that the antibonding band narrows and loses intensity as $|\Delta/t|$ is increased.

In the Γ -K cut (Fig. 12) we see that the bonding band moves from the Fermi level at $\Delta = 0$ to lower energies such that it is completely filled at larger values of $|\Delta/t|$. At first sight Fig. 12 might appear to suggest that the bonding band also narrows as $|\Delta/t|$ increases, however it is clear from Fig. 11 that this is not the case. Rather, as $|\Delta/t|$ increases the system becomes more one dimensional (for $t/\Delta = 0$, the system consists of uncoupled one-dimensional chains), increasing the range of $E_{\mathbf{k}}$ in the cuts shown in Fig. 11 and decreasing the range of $E_{\mathbf{k}}$ in the cuts shown in Fig. 12 (cf. Figs. 5 and 9).

D. Quantum oscillations

As we are considering a quasi-two-dimensional metal the cyclotron effective mass, m_{\pm} , associated with Shubnikov-de Haas oscillations of the part of the Fermi surface arising from the \pm band is⁵⁹

$$m_{\pm} = 2\pi\hbar^2 D_{\pm}(E_F), \quad (24)$$

where $D_{\pm}(E_F)$ is the renormalised density of states per spin at the Fermi energy, E_F , arising from the \pm band.

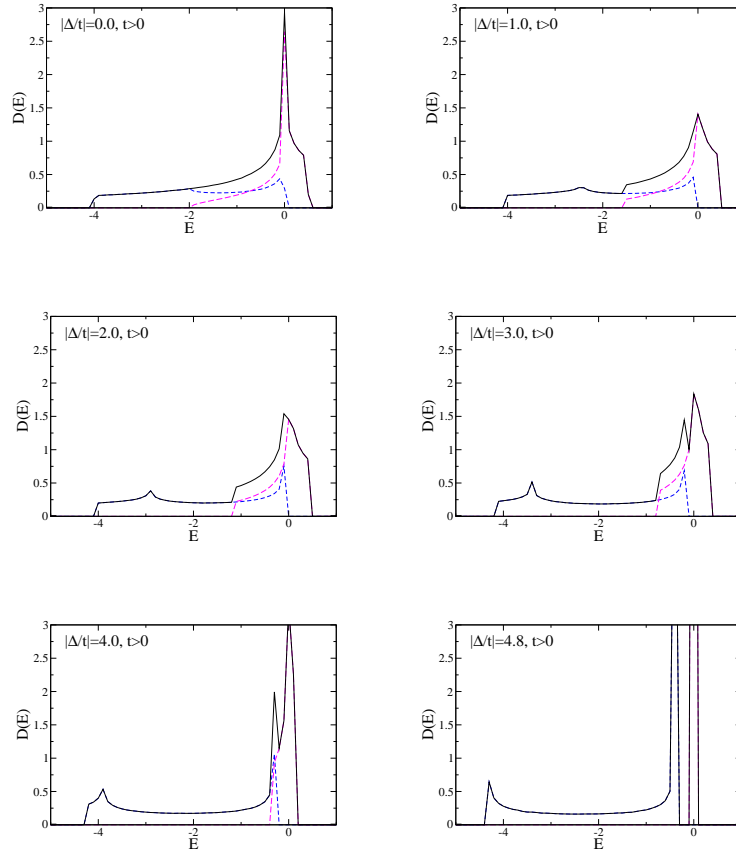


FIG. 8: [Color online] Density of states (in units where $|t| = a = 1$) of the fermions for $t > 0$. Dashed (blue and pink) lines indicate the contributions of the individual bands. As in Fig. 7 we see that the antibonding band rapidly narrows at $|\Delta/t|$ increases. Furthermore, the width of the bonding band is almost independent of $|\Delta/t|$. Again, the DOS is very different from the non-interacting case, cf. Fig. 19, particularly for large $|\Delta/t|$. Also see the online movie.⁵⁷

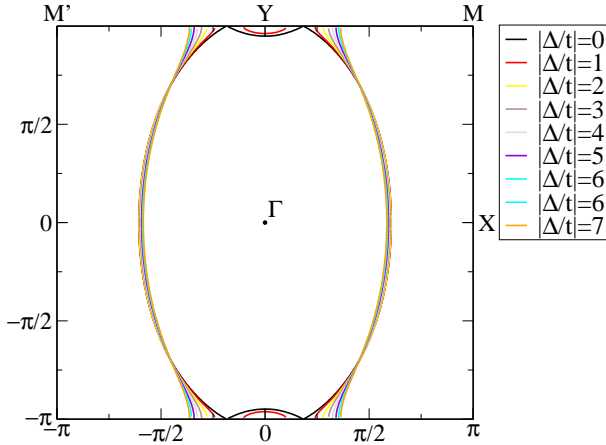


FIG. 9: [Color online] Fermi surface of the fermions for $t < 0$. For small $|\Delta/t|$ there are small Fermi pockets around the Y points. Comparing the Fermi surface with the band structure of the fermions shows that these pockets arise from the bonding band. One therefore expects that these fermions are lighter than those in the quasi-one-dimensional sheets, which arise from the antibonding band (cf. Fig. 13). The Brillouin zone is that of the ionic Hubbard model (cf. Fig. 1e).

We plot the variation of the cyclotron mass with $|\Delta/t|$ for parameters relevant to $\text{Na}_{0.5}\text{CoO}_2$, i.e., $t = -0.1$ eV, a basal lattice constant, $a = 2.82$ Å, and a unit cell basal area of $\sqrt{3}a \times 2a$, in Fig. 13. The cyclotron mass for the bonding band associated with the small pockets is about one quarter of that for heavy electrons associated with the antibonding band.

In order to observe the states arising from the antibonding band, i.e., the quasi-1D sheets on the Fermi surface, in quantum oscillation experiments a field that is sufficiently large to cause magnetic breakdown between the two bands must be applied. The field required for magnetic breakdown and the large effective mass associated the antibonding band make it more difficult to observe the breakdown orbit than the small pockets in quantum oscillation experiments.

For realistic parameters for $\text{Na}_{0.5}\text{CoO}_2$, $\Delta \sim |t| \ll U$ and $t < 0$ (cf. section IB), the slave boson theory presented above suggests that the system is metallic. However, an important question, which we cannot conclusively answer because of the uncertainty in the precise value of $|\Delta/t|$ relevant to $\text{Na}_{0.5}\text{CoO}_2$, is: is $|\Delta/t|$ large enough in $\text{Na}_{0.5}\text{CoO}_2$ that the bonding band is completely filled? For $|\Delta/t| < 1.5$ there are two features

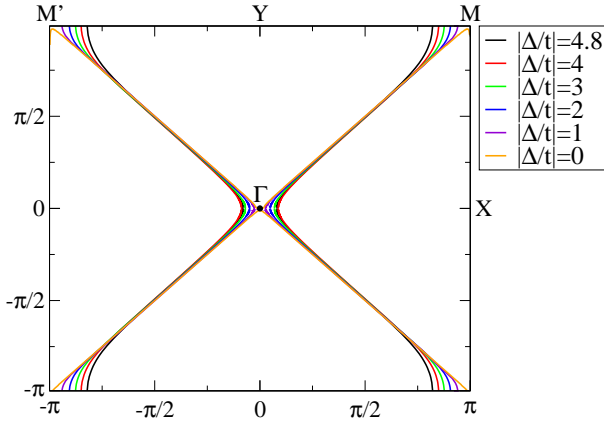


FIG. 10: [Color online] Fermi surface of the fermions for $t > 0$. For $t > 0$ the bonding band is always completely filled. Therefore this Fermi surface arises entirely from the antibonding band. As $|\Delta/t|$ is increased only rather subtle changes are observed in the Fermi surface, most notably, the nesting is slightly decreased. The Brillouin zone is that of the ionic Hubbard model (cf. Fig. 1e).

in the Fermi surface (cf. Fig. 9): small hole-like pockets of light fermions arising from the bonding (nearly filled) band, and quasi-one-dimensional sheets of heavier electron-like quasiparticles. This seems to be quite consistent with quantum oscillations,⁷ which are observed to have a frequency correspond to orbits that encompass less than 1% of the first Brillouin zone, in apparent violation of Luttinger's theorem. A natural explanation of this experiment is that Balicas *et al.*⁷ are only able to observe the, small, light, quasiparticles in the bonding band and do not see oscillations arising from the antibonding band, either because the quasiparticles in the antibonding band are too heavy, or because the field they applied is insufficient to cause magnetic breakdown of the 'gap' between the quasi-one-dimensional sheets and the two-dimensional pockets. However, for $|\Delta/t| > 1.5$ the small Fermi pockets are absent as the bonding band is filled, and our results would be inconsistent with the quantum oscillations observed by Balicas *et al.*

E. A picture of $\text{Na}_{0.5}\text{CoO}_2$

The experimental situation, particularly in $\text{Na}_{0.5}\text{CoO}_2$, is somewhat confusing. Several experiments suggest an insulating state: resistivity versus temperature has a negative gradient at low temperatures,⁴ and angle resolved photoemission spectroscopy (ARPES)⁶ and optical conductivity⁵ both observe a gap, all of which suggests that below 51 K $\text{Na}_{0.5}\text{CoO}_2$ is an insulator. However, quantum oscillations are observed,⁷ which suggest that there are quasiparticles and that the system is metallic with a small Fermi surface (occupying less than 1% of the cross-sectional area of the first Brillouin zone) and an effective mass similar to the free electron mass.

Below we propose a picture, inspired by both the mean field slave boson theory (above) and our previous exact diagonalisation calculations for the same ionic Hubbard model,^{23,24} that offers a possible reconciliation of these seemingly contradictory experiments. However, it is important to stress that this is a tentative proposal and does not correspond to the solution found in either theory. Nevertheless, we will argue, below, that this picture is plausible given the limitations of the mean field slave boson theory and the finite size effects in the exact diagonalization calculations. Further calculations will be required to discover whether this proposal is indeed supported by the theory of the ionic Hubbard model.

The fundamental definition of a metal is a substance with charge carrying excitations at arbitrarily low energies above the ground state. In most situations it follows that the resistivity monotonically increases with temperature as increasing the temperature decreases the quasiparticle lifetime. However, this is not necessarily the case. For example, in many strongly correlated systems, such as the organic superconductors,⁶⁰ the charge transport is incoherent at high temperatures - this leads to a resistivity with a broad maximum slightly above the temperature where quasiparticle coherence is lost.⁶¹ Above, we have shown that the slave boson theory of Hamiltonian (2) produces two bands. We will assume some features of these bands survive even in the exact solution even if the simple single particle states, of the slave boson theory, do not. The antibonding band is narrow and it is likely that coherent quasiparticles do not emerge from these states until quite low temperatures. Within slave boson theories the coherence temperature can be estimated from the Bose condensation temperature, T_B of the slave bosons,⁵² which, in 2D, is proportional to the density of bosons, ρ_B . For $|\Delta/t| \rightarrow 0$ there are 0.993 quasiholes per unit cell in the antibonding band, corresponding to $\rho_B = 0.007$, and the density of bosons decreases as $|\Delta/t|$ is increased, going to zero at $|\Delta/t|=1.5$. Estimating the Bose condensation temperature (cf. Refs. 52 and 62) by either $T_B \approx (2\pi\rho_B)/(\sqrt{3}a^2m_B)$, where a is the basal plane lattice constant (2.82 Å for $\text{Na}_{0.5}\text{CoO}_2$) and $m_B \approx 2m$ is the mass of the boson (which is the simplest approximation given that the boson corresponds to two electrons), or $T_B \approx 4\pi\rho_B t$ yields $T_B \sim 100$ K for $\rho_B = 0.007$. However it is well known that these simple formulae dramatically overestimate the coherence temperature as they neglect gauge fluctuations.^{52,62} Thus the coherence temperature ($T^* \ll 100$ K) is expected to be extremely low in the experimentally relevant parameter regime.

This low coherence temperature is consistent with the observed incoherent transport evident from the resistivity above ~ 51 K. As the temperature is lowered below 51 K the resistivity rises rapidly, suggesting that a gap opens. The slave boson calculations do not predict a true gap unless $|\Delta/t| \gg 1$. Experiments observe magnetic ordering,^{26,31,37,41} which we have not considered here, below 88 K, but, as the gap does not appear to

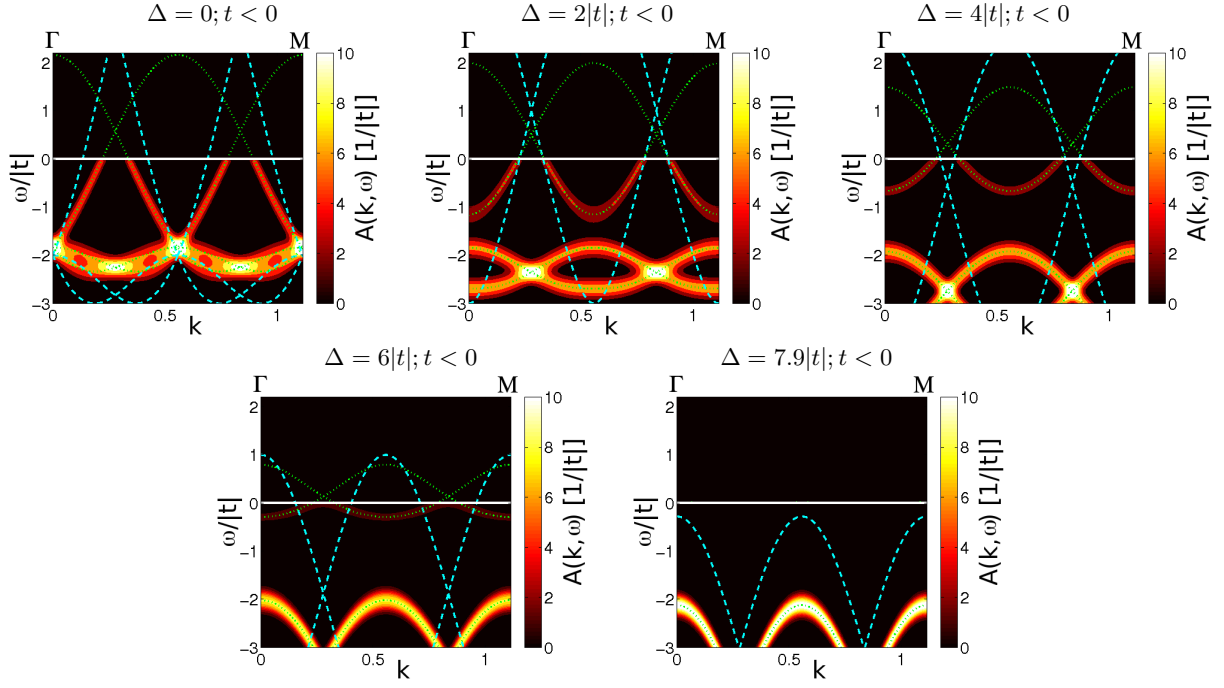


FIG. 11: [Color online] Cut of the spectral density, $A(\mathbf{k}, \omega)$, along the Γ -M direction of the triangular lattice Brillouin zone (cf. Fig. 1d). $A(\mathbf{k}, \omega)$ is calculated from Eq. (18), broadened as described in the text below Eq. (23), and plotted for $k_B T = |t|/60 \simeq 20$ K. Green dotted lines are the slave boson dispersion, blue dashed lines are the bare dispersion. The abscissa is in \AA^{-1} , with the lattice constant taken as $a = 2.82$ \AA , as is appropriate for $\text{Na}_{0.5}\text{CoO}_2$.⁹ As $|\Delta/t|$ is increased the spectral weight is transferred from the antibonding band to the bonding band and the antibonding band narrows. Also see the online movie.⁵⁷

open until 51 K, one cannot conclude that the magnetic order causes the gap to open. However, previous exact diagonalisation calculations^{23,24} suggest that in the experimentally relevant parameter regime, $-t \sim \Delta \ll U$, non-local correlations, not captured by our mean field treatment, drive the formation of a covalent insulator. We propose that a gap opens on the antibonding band at 51 K due to non-local correlations, analogous to the covalent insulator. But, we also propose that the bonding band remains ungapped.

This proposal is rather similar to the theory of the orbital-selective Mott transition. The question of whether, in multi-band systems, one band can become insulating, due to electronic correlations, while others remain metallic has been extensively discussed recently,⁶³ motivated, in part, by the volume collapse in Ce (Ref. 64), the heavy fermion behaviour of $\text{Ca}_{2-x}\text{Sr}_x\text{RuO}_4$ (Ref. 65) and the nodal-anti-nodal differentiation in the cuprates.⁶⁶ Although the debate is ongoing, the current theoretical consensus is that orbital-selective Mott transitions can occur for some parameter regimes of some models.⁶³ Therefore, testing our proposed picture will require calculations beyond the mean-field slave-boson theory presented above.

Given the important differences between the current mean field calculations and our previous exact diagonalisation calculations, particularly the critical value of $|\Delta/t|$ for the metal-insulator transition, it is important

to ask, whether this explanation is likely to hold in the exact solution and, more importantly, for the real material. Firstly, we note that the real space charge disproportionation calculated from our mean field theory is in very good agreement with exact diagonalisation calculations in the experimentally relevant regime. This gives one hope that the filling of the bands calculated from the mean field theory may also be reasonable (although non-local Coulomb correlations could cause additional hybridisation effects, cf. Ref. 24). Secondly, we note that the finite size clusters that were, necessarily, studied in the exact diagonalisation calculations mean that it is extremely difficult to accurately study the bonding band. Taking a typical, 18 site (9 unit cell) cluster, a density of 0.007 holes per unit cell means that one would expect less than $1/16^{\text{th}}$ of a hole in the bonding band in the exact diagonalisation calculation. However, exact diagonalisation calculations do accurately reproduce the band filling of the analytical exact solution for $U = 0$.^{23,24} Therefore, it is not clear, at present, whether the exact diagonalisation calculations can resolve the tiny hole pockets suggested by our calculations and the quantum oscillation experiments.

As the exact diagonalisation calculations do not rule out the possibility that small weakly correlated Fermi pockets containing a tiny number of charge carriers remain even in the low temperature ‘insulating’ state, let us briefly discuss how this would produce a consistent

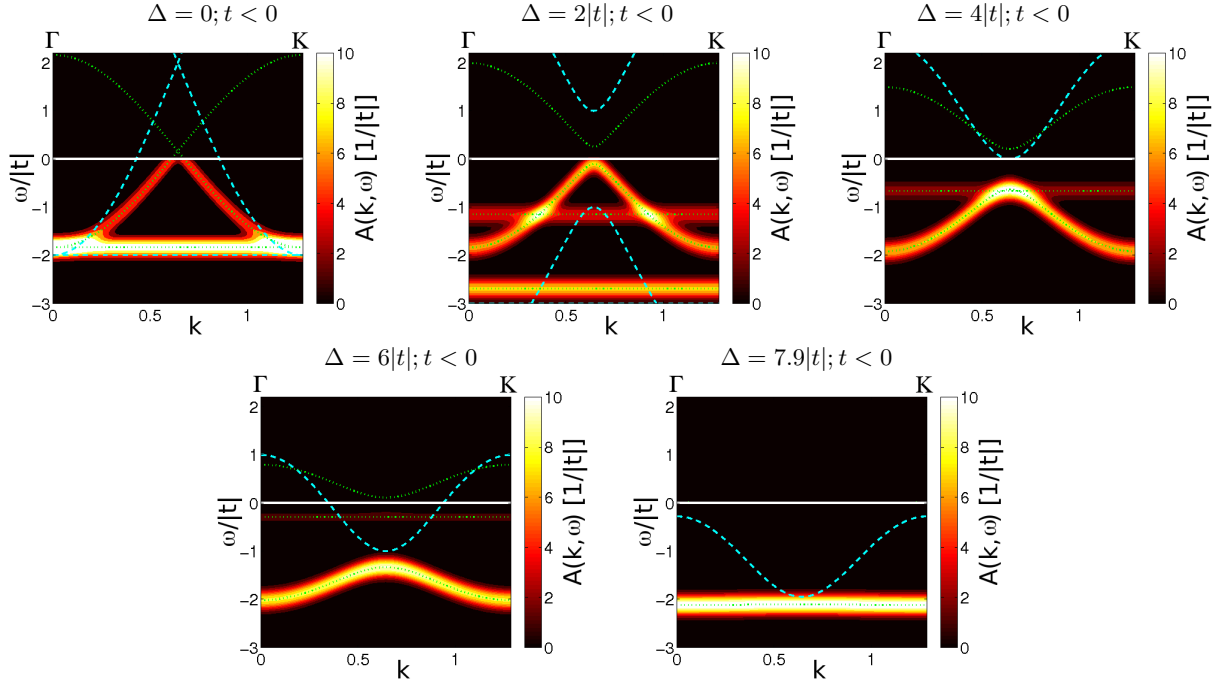


FIG. 12: [Color online] Cut of the spectral density, $A(\mathbf{k}, \omega)$, along the Γ -K direction of the triangular lattice Brillouin zone (cf. Fig. 1d). $A(\mathbf{k}, \omega)$ is calculated from Eq. (18), broadened as described in the text below Eq. (23), and plotted for $k_B T = |t|/60 \simeq 20$ K. Green dotted lines are the slave boson dispersion, blue dashed lines are the bare dispersion. The abscissa is in \AA^{-1} , with the lattice constant taken as $a = 2.82 \text{ \AA}$, as is appropriate for $\text{Na}_{0.5}\text{CoO}_2$.⁹ At small $|\Delta/t|$ the bonding band crosses the Fermi energy in this direction (cf. Figs. 5 and 9). As $|\Delta/t|$ is increased the bonding band is pushed below the Fermi energy and spectral weight is transferred from the antibonding band to the bonding band, which is not dispersive in this direction. Also see the online movie.⁵⁷

explanation of the experiments on $\text{Na}_{0.5}\text{CoO}_2$.

It is important to note that the two bands act as parallel channels for charge transport. Above 51 K charge transport in the antibonding band will be incoherent (assuming the coherence temperature < 50 K, as we have argued above) and the resistivity in this channel can be estimated to be $\gtrsim \hbar c/e^2$, where c is the interlayer spacing, i.e., at or above the Mott-Ioffe-Regel limit. Below 51 K a gap opens on the antibonding band, but as the gap is small, $\mathcal{O}(t)$ (Ref. 23,24) the resistivity in the antibonding channel is not increased by orders of magnitude from the resistivity value in the incoherent metallic state. However, because of the extremely low charge carrier concentration in the bonding band (metallic channel) the contribution of the bonding band to the conductivity will be even smaller than that of the antibonding band (incoherent/insulating channel). Therefore the metallic channel will be unable to ‘short circuit’ the incoherent/insulating channel. This contention is supported by the fact that even above 51 K the resistivity is larger than the Mott-Ioffe-Regel limit. Thus the observation that the resistivity decreases with increasing temperature is not necessarily inconsistent with the observation of quasiparticles in quantum oscillation experiments.

Foo *et al.*⁴ found that the conductivity, σ , of $\text{Na}_{0.68}\text{CoO}_2$ is very similar to that of $\text{Na}_{0.31}\text{CoO}_2$ and that both of these are an order of magnitude larger than

the conductivity of $\text{Na}_{0.5}\text{CoO}_2$. As $\sigma \propto n$, one expects that the contribution of the electrons in the bonding band to the conductivity of $\text{Na}_{0.5}\text{CoO}_2$ will be two orders of magnitude smaller than the total conductivity of $\text{Na}_{0.68}\text{CoO}_2$ or $\text{Na}_{0.31}\text{CoO}_2$. Therefore Foo *et al.*’s results are consistent with the, counterintuitive, picture that the insulating band short-circuits the metallic band!

ARPES, which measures $A(\mathbf{k}, \omega)$, has been reported in the directions Γ -M and Γ -K, i.e., in the directions of the cuts shown in Figs. 11 and 12 respectively. However, our slave boson calculations do not capture the gap on the antibonding band required in our proposal. Therefore the gap observed in the ARPES is likely to correspond to the ‘covalent insulator’ gap on the antibonding band. Optical conductivity does not observe a Drude peak, however the height of the Drude peak is proportional to the charge carrier density, which would make the tiny Fermi pockets suggested by our slave boson calculations difficult to observe.

As one expects that the Fermi pockets do not contribute significantly to either the resistivity or the Hall coefficient the correspondence of our mean-field slave boson theory to the empirical low energy Hamiltonian studied by Choy *et al.*⁴² (discussed in section II C) become important. The non-local correlations on the antibonding band open up a gap on the quasi-one-dimensional sheets of the Fermi surface. This provides the gap assumed by

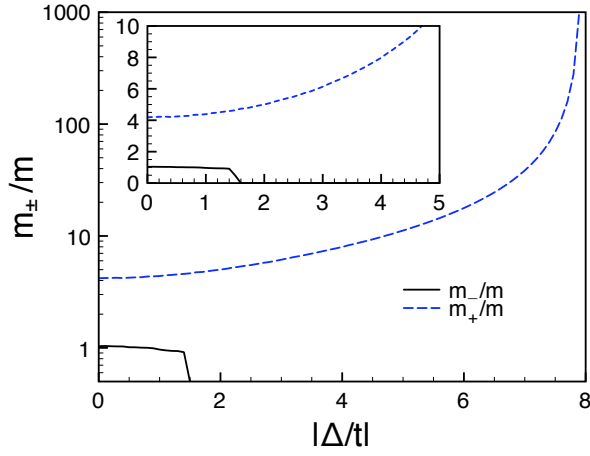


FIG. 13: [Color online] Variation of the renormalised cyclotron effective mass, m_{\pm} , in units of the free electron mass, m , with $|\Delta/t|$ for $t < 0$. Note that in the main panel the ordinate is plotted on a logarithmic scale: the same data is plotted on a linear scale in the inset. $m_-/m \sim 1$ and $m_+/m \sim 4$ for small $|\Delta/t|$. The cyclotron effective mass of the antibonding band diverges as the metal-charge transfer insulator transition is approached, consistent with our finding that the metal-charge ordered insulator transition is second order, cf. Fig. 3. The cyclotron effective masses are calculated from Eq. (24) with parameters appropriate for $\text{Na}_{0.5}\text{CoO}_2$: $t = -0.1$ eV, an in-plane lattice constant, $a = 2.82$ Å, and a unit cell basal area of $\sqrt{3}a \times 2a$.

Choy *et al.* and suggests that their results will carry across to our model. This suggests that the measured temperature dependence of both the resistivity and the Hall coefficient in $\text{Na}_{0.5}\text{CoO}_2$ have a natural explanation in terms of the ionic Hubbard model. However, clearly further calculations are required to test the validity of this *ad hoc* proposal and its relevance to $\text{Na}_{0.5}\text{CoO}_2$.

IV. SUMMARY AND CONCLUSIONS

We have presented a mean-field slave boson theory of the ionic Hubbard model on the triangular lattice with alternating stripes of site energy. This model has two bands: one of which is weakly correlated and nearly filled or filled, the other is nearly half-filled or half-filled and hence strongly correlated. The results depend strongly on the sign of t . The light band is always filled for $t > 0$, but only becomes filled at $|\Delta/t| = 1.5$ for $t < 0$. A metal-charge transfer insulator transition occurs at larger $|\Delta/t|$ (5.0 for $t > 0$ and 8.0 for $t < 0$), when complete charge disproportionation occurs and one sublattice is filled and the other in half filled.

We have also proposed a speculative picture of $\text{Na}_{0.5}\text{CoO}_2$. In particular, we have argued that the observed quantum oscillations arise from quasiparticles in the bonding band, but these are not seen in the zero field resistivity and several other experiments because the

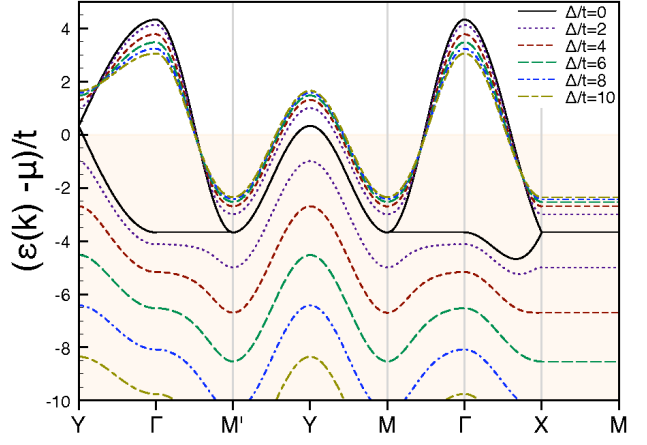


FIG. 14: Band structure of the ionic Hubbard model for $U = 0$, at three-quarters filling, and $t < 0$. Increasing $|\Delta/t|$ makes the system increasingly anisotropic, which serves to flatten the bands slightly in some directions. The constraint of three quarters filling ‘pins’ the antibonding band to the Fermi energy, but increasing $|\Delta/t|$ pushes the bonding band to lower energies.

low density of charge carriers in the bonding band mean that the metallic bonding band is not able to ‘short circuit’ the incoherent/insulating antibonding band. Calculations beyond the mean field slave boson calculations, which we have presented above, will be required to test this picture.

Another important avenue for future work will be to allow for magnetic ordering in the theory as this may improve the degree of agreement with experiments and allow one to compare with other experiments such as NMR^{26,41} and neutron scattering.^{31,37}

Acknowledgements

We thank H. Alloul, J. Bobroff, M.-H. Julien, and R. P. Singh for helpful discussions. Numerical calculations were performed on the Australian Partnership for Advanced Computing national facility under the a grant from the merit allocation scheme. This work was supported by the Australian Research Council (ARC) under the discovery program (project numbers DP0557532 and DP0878523), MEC (project CTQ2005-09385-C03-03) and MICINN (project CTQ2008-06720-C02-02). B. J. P. was supported by the ARC under the Queen Elizabeth II scheme (DP0878523). J. M. acknowledges financial support from the Ramón y Cajal program. R.H.M. was supported by the ARC under the APF scheme (DP0877875).

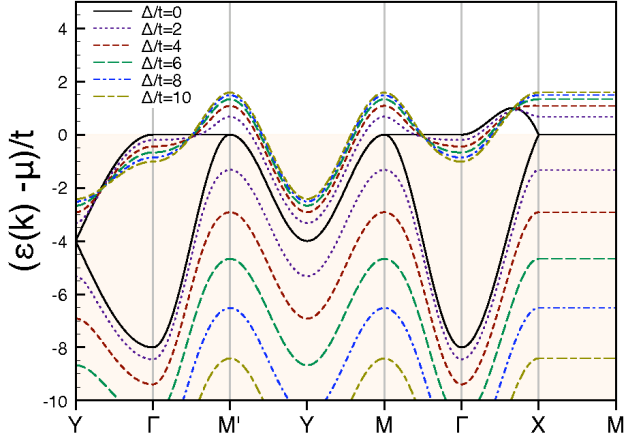


FIG. 15: Band structure of the ionic Hubbard model for $U = 0$, at three-quarters filling, and $t > 0$. This band structure is markedly different from the $t < 0$ case (Fig. 14). This is consistent with the general expectation that particle-hole symmetry is absent on frustrated lattices and hence that the sign of t has strong effects on the physics.

APPENDIX A: NON-INTERACTING ELECTRONS

For $U = 0$ there are two bands, bonding (-) and anti-bonding (+), and whose dispersion relations are

$$\varepsilon_{\mathbf{k}}^{\pm} = -2t \cos(k_x) \pm \sqrt{\Delta^2/4 + (4t \cos(k_x/2) \cos(k_y/2))^2}, \quad (\text{A1})$$

where k_x and k_y are defined in the reduced $(1 \times \sqrt{3})$ Brillouin zone of Hamiltonian (2), shown in Fig. 1e. These dispersion relations are plotted in Figs. 14 and 15 for $t < 0$ and $t > 0$ respectively.

To calculate where the bonding band becomes filled we need to consider the maximum of $\varepsilon_{\mathbf{k}}^-$. This is complicated by the fact the chemical potential, μ , is a function of Δ . For $t > 0$ the top of the bonding band is at $\varepsilon_X^- = \varepsilon_M^- = \varepsilon_{(\pi,y)}^-$. Thus we find that the bonding band become full at $\Delta \geq \Delta^> \equiv 2\mu(\Delta^>) + 4|t|$. However, for $\Delta = 0^+$ or 0^- and $t > 0$ one finds that $\mu = -2.0t$ and this condition is satisfied. Therefore the bonding band is filled, and hence the antibonding band is half filled, for an infinitesimal Δ . Note that this is not the case for $\Delta = 0$ as we require at least an infinitesimal Δ to double the size of the unit cell and cause the splitting into two bands, cf. Figs. 1a and 1b. For $t < 0$ the top of the bonding band is ε_Y^- and we find the bonding band is filled for $\Delta \geq \Delta^< \equiv 2\mu(\Delta^<) + 4|t|$. Solving this condition numerically we find that $\Delta^< = -0.64|t|$.

In Figs. 16 and 17 we plot the Fermi surfaces for non-interacting electrons for each sign of t at a range of $|\Delta/t|$. The first point to note is that at low $|\Delta/t|$ the two Fermi surfaces are very different. As $|\Delta/t| \rightarrow \infty$ both Fermi

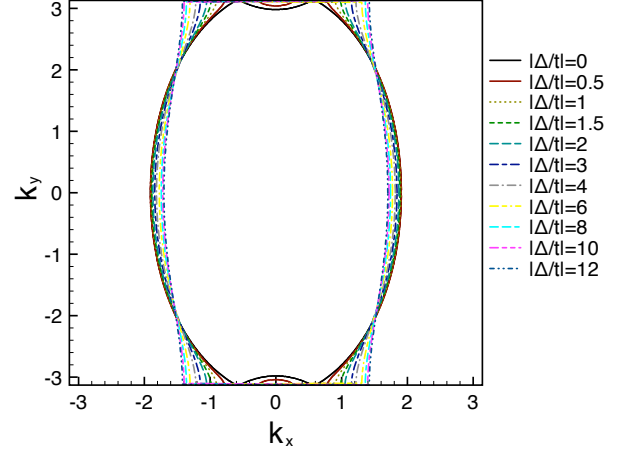


FIG. 16: [Color online] Fermi surface for non-interacting electrons for $t < 0$. For small $|\Delta/t|$ there are small Fermi pockets around the Y points. As $|\Delta/t|$ is increased the Fermi surface becomes increasingly quasi-one-dimensional.

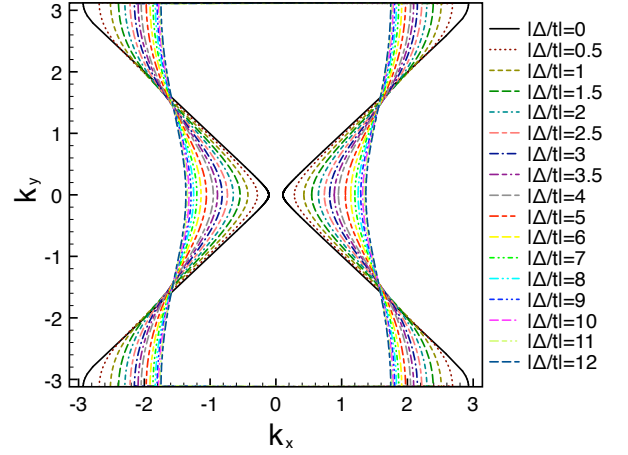


FIG. 17: [Color online] Fermi surface for non-interacting electrons for $t > 0$. For $t > 0$ the bonding band is always completely filled. Therefore this Fermi surface arises entirely from the antibonding band. Note that the Fermi surface is very different from that for $t < 0$ (Fig. 16).

surfaces become quasi-one-dimensional; but, even in this limit the two Fermi surfaces are different in important ways as for $t < 0$ the Fermi surface is electron like, while of $t > 0$ the Fermi surface is hole like. Only when we reach the limit, and both Fermi surfaces are straight lines, are the two Fermi surfaces the same.

We plot the DOS of the non-interacting ($U = 0$) system in Figs. 18 and 19 for $t < 0$ and $t > 0$ respectively. Notice that the plots are very different for the two different signs of t . In particular at $\Delta = 0$ the Fermi energy is at the van Hove singularity for $t > 0$, but is not for $t < 0$. This suggests that the Fermi liquid will be less stable for $t > 0$ than for $t < 0$. Indeed we find that, in the slave boson theory, the MIT occurs at $|\Delta/t| = 5.0$ for $t > 0$ and $|\Delta/t| = 8.0$ for $t < 0$, consistent with this expectation

(cf. Fig. 2). However, as $|\Delta/t|$ is increased the van Hove singularity is moved away from the Fermi energy even for

$t > 0$, so this, weak coupling, description is clearly not the whole story of the strong coupling theory.

-
- * Electronic address: bjpowell@gmail.com
- ¹ See, for example, N. P. Ong and R. J. Cava, *Science* **305**, 52 (2004).
 - ² J. Merino, B. J. Powell, and R. H. McKenzie, *Phys. Rev. B* **73**, 235107 (2006).
 - ³ K. Takada *et al.*, *Nature* **422**, 53 (2003).
 - ⁴ M. L. Foo, Y. Wang, S. Watauchi, H.W. Zandbergen, T. He, R. J. Cava, and N. P. Ong, *Phys. Rev. Lett.* **92**, 247001 (2004).
 - ⁵ N.L. Wang *et al.*, *Phys. Rev. Lett.* **93**, 147403 (2004); J. Hwang *et al.*, *Phys. Rev. B* **72**, 024549 (2005); S. Lupi *et al.*, *Phys. Rev. B* **72**, 024550 (2005).
 - ⁶ D. Qian, L. Wray, D. Hsieh, D. Wu, J. L. Luo, N. L. Wang, A. Kuprin, A. Fedorov, R. J. Cava, L. Viciu, and M. Z. Hasan, *Phys. Rev. Lett.* **96**, 046407 (2006).
 - ⁷ L. Balicas, M. Abdel-Jawad, N. E. Hussey, F. C. Chou, and P. A. Lee, *Phys. Rev. Lett.* **94**, 236402 (2005).
 - ⁸ M. Z. Hasan, Y.-D. Chuang, D. Qian, Y. W. Li, Y. Kong, A. P. Kuprin, A. V. Fedorov, R. Kimmerling, E. Rotenberg, K. Rossnagel, Z. Hussain, H. Koh, N. S. Rogado, M. L. Foo, and R. J. Cava, *Phys. Rev. Lett.* **92**, 246402 (2004); H.-B. Yang, S.-C. Wang, A. K. P. Sekharan, H. Matsui, S. Souma, T. Sato, T. Takahashi, T. Takeuchi, J. C. Campuzano, R. Jin, B. C. Sales, D. Mandrus, Z. Wang, and H. Ding, *ibid.* **92**, 246403 (2004).
 - ⁹ P. Zhang, R. B. Capaz, M. L. Cohen, S. G. Louie, *Phys. Rev. B* **71**, 153102 (2005).
 - ¹⁰ M. Roger, D. J. P. Morris, D. A. Tennant, M. J. Gutmann, J. P. Goff, J. U. Hoffmann, R. Feyerherm, E. Dudzik, D. Prabhakaran, A. T. Boothroyd, N. Shannon, B. Lake, and P. P. Deen, *Nature* **445**, 631 (2007).
 - ¹¹ H. W. Zandbergen, M. L. Foo, Q. Xu, V. Kumar, and R. J. Cava, *Phys. Rev. B* **70**, 024101 (2004).
 - ¹² T. Egami, S. Ishihara, and M. Tachiki, *Science* **261**, 1307 (1993).
 - ¹³ A. P. Kampf, M. Sekania, G. I. Japaridze, and Ph. Brune, *J. Phys.: Condens. Matter* **15**, 5895 (2003); also see references therein and citations thereof for further details of the extensive literature on the ionic Hubbard model in one-dimension.
 - ¹⁴ A. Garg, H. R. Krishnamurthy, and M. Randeria, *Phys. Rev. Lett.* **97**, 046403 (2006).
 - ¹⁵ L. Craco, P. Lombardo, R. Hayn, G. I. Japaridze, and E. Müller-Hartmann, *Phys. Rev. B* **78**, 075121 (2008).
 - ¹⁶ S. S. Kancharla and E. Dagotto, *Phys. Rev. Lett.* **98**, 016402 (2007).
 - ¹⁷ N. Paris, K. Bouadim, F. Hebert, G. G. Batrouni, and R. T. Scalettar, *Phys. Rev. Lett.* **98**, 046403 (2007).
 - ¹⁸ K. Bouadim, N. Paris, F. Hébert, G. G. Batrouni, and R. T. Scalettar, *Phys. Rev. B* **76**, 085112 (2007).
 - ¹⁹ K. Penc, H. Shiba, F. Mila, and T. Tsukagoshi, *Phys. Rev. B* **54**, 4056 (1996).
 - ²⁰ G. I. Japaridze, R. Hayn, P. Lombardo, E. Müller-Hartmann, *Phys. Rev. B* **75**, 245122 (2007).
 - ²¹ K. Byczuk, M. Ulmke, and D. Vollhardt, *Phys. Rev. Lett.* **90**, 196403 (2003).
 - ²² C. A. Marianetti and G. Kotliar, *Phys. Rev. Lett.* **98**, 176405 (2007).
 - ²³ J. Merino, B. J. Powell, and R. H. McKenzie, *Phys. Rev. B* **79**, 161103(R) (2009).
 - ²⁴ J. Merino, R. H. McKenzie, and B. J. Powell, *arXiv:0904.3402*.
 - ²⁵ F.L. Ning *et al.*, *Phys. Rev. Lett.* **93**, 237201 (2004).
 - ²⁶ J. Bobroff *et al.*, *Phys. Rev. Lett.* **96**, 107201 (2006).
 - ²⁷ A. J. Williams *et al.*, *Phys. Rev. B* **73**, 134401 (2006); D. Argyriou *et al.*, *Phys. Rev. B* **76**, 134506 (2007).
 - ²⁸ F.L. Ning *et al.*, *Phys. Rev. Lett.* **100**, 086405 (2008).
 - ²⁹ G. Garbarino *et al.*, *Rev. B* **77**, 064105 (2008).
 - ³⁰ The dependence on the direction of the field may be explained by (i) the larger g-factor for fields parallel to the layers, and/or (ii) that the transitions at 51 K and 88 K have a larger effect on the bulk magnetic susceptibility parallel to the layers, χ_{ab} than on χ_c (see Fig. 1(c) in Ref. 31 and Fig. 8 in Ref. 32).
 - ³¹ G. Gasparovic *et al.*, *Phys. Rev. Lett.* **96**, 046403 (2006).
 - ³² H. Watanabe *et al.*, *J. Phys. Soc. Jap.* **75**, 034716 (2006).
 - ³³ P. Mendels, D. Bono, J. Bobroff, G. Collin, D. Colson, N. Blanchard, H. Alloul, I. Mukhamedshin, F. Bert, A. Amato, and A. D. Hillier, *Phys. Rev. Lett.* **94**, 136403 (2005).
 - ³⁴ I.R. Mukhamedshin, H. Alloul, G. Collin, and N. Blanchard, *Phys. Rev. Lett.* **94**, 247602 (2005).
 - ³⁵ M.-H. Julien, C. de Vaulx, H. Mayaffre, C. Berthier, M. Horvatić, V. Simonet, J. Wooldridge, G. Balakrishnan, M. R. Lees, D. P. Chen, C. T. Lin, and P. Lejay, *Phys. Rev. Lett.* **100**, 096405 (2008).
 - ³⁶ H. Alloul, I.R. Mukhamedshin, G. Collin, and N. Blanchard, *Europhys. Lett.* **82**, 17002 (2008).
 - ³⁷ M. Yokoi, T. Moyoshi, Y. Kobayashi, M. Soda, Y. Yasui, M. Sato, and K. Kakurai, *J. Phys. Soc. Jpn.* **74**, 1800 (2005).
 - ³⁸ H. Alloul, I.R. Mukhamedshin, T.A. Platova, and A.V. Dooglav, *Europhys. Lett.* **85**, 47006 (2009).
 - ³⁹ G. Lang, J. Bobroff, H. Alloul, G. Collin, and N. Blanchard, *Phys. Rev. B* **78**, 155116 (2008).
 - ⁴⁰ J. Bobroff *et al.*, *Phys. Rev. B* **76**, 100407(R) (2007).
 - ⁴¹ T. F. Schulze *et al.*, *Phys. Rev. Lett.* **100**, 026407 (2008).
 - ⁴² T.-P. Choy, D. Galanakis, and P. Phillips, *Phys. Rev. B* **75**, 073103 (2007).
 - ⁴³ K.-W. Lee, J. Kuneš, P. Noval, and W. E. Pickett, *Phys. Rev. Lett.* **94**, 026403 (2005).
 - ⁴⁴ K.-W. Lee and W. E. Pickett, *Phys. Rev. Lett.* **96**, 096403 (2006).
 - ⁴⁵ S. Zhou and Z. Wang, *Phys. Rev. Lett.* **98**, 226402 (2007).
 - ⁴⁶ K.-W. Lee and W. E. Pickett, *Phys. Rev. B* **76**, 134510 (2007).
 - ⁴⁷ S. Landron and M.-B. Lepetit, *arXiv:0805.3121*.
 - ⁴⁸ D. J. Singh, *Phys. Rev. B* **61**, 13397 (2000).
 - ⁴⁹ C. de Vaulx, M.-H. Julien, C. Berthier, S. Hébert, V. Pralong, and A. Maignan, *Phys. Rev. Lett.* **98**, 246402 (2007).
 - ⁵⁰ M. Capone, L. Capriotti, F. Becca, and S. Caprara, *Phys. Rev. B* **63**, 085104 (2001).
 - ⁵¹ S. E. Barnes, *J. Phys. F* **6**, 1375 (1976); *ibid.* **7**, 2637 (1977); P. Coleman, *Phys. Rev. B* **29**, 3035 (1984).

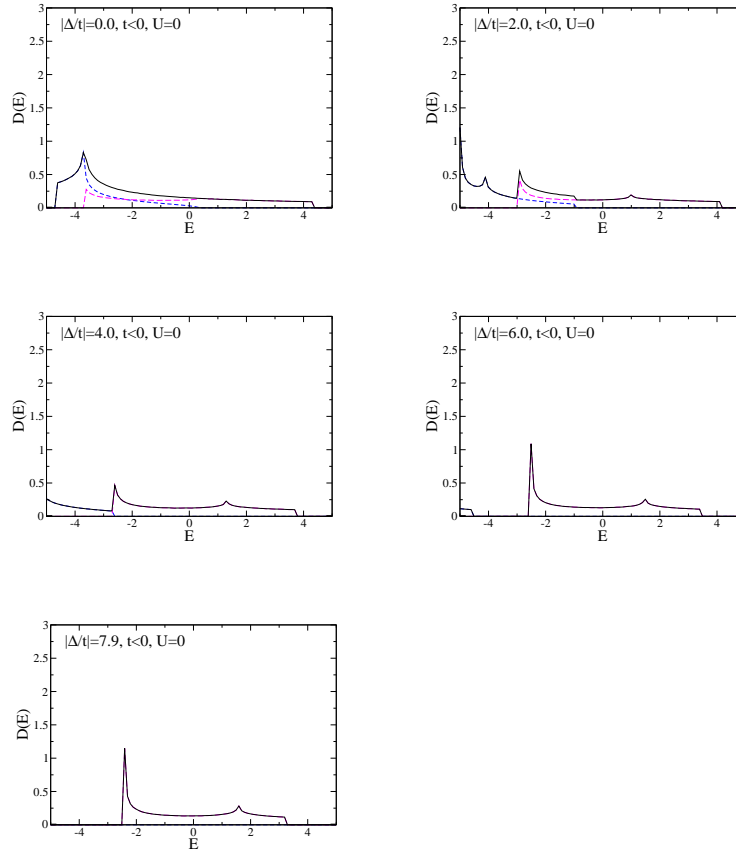


FIG. 18: [Color online] Density of states for $U = 0$ and $t < 0$. Dashed (blue and pink) lines indicate the contributions of the individual bands.

- ⁵² P. A. Lee, N. Nagaosa, and X.-G. Wen, *Rev. Mod. Phys.* **78**, 17 (2006).
- ⁵³ See, for example, section 4.10 of M. L. Boas *Mathematical methods in the physical sciences* (2nd edition, Wiley, New York, 1983).
- ⁵⁴ J. Spalek and W. Wójcik, in *Spectroscopy of the Mott Insulators and Correlated Metals*, Springer Series in Solid State Sciences Vol. 119 (Springer-Verlag, Berlin, 1995), pp. 41-65.
- ⁵⁵ S. Burdin, A. Georges, and D. R. Grempel, *Phys. Rev. Lett.* **85**, 1048 (2000).
- ⁵⁶ D. D. Sarma, *J. Sol. State Chem.* **88**, 45 (1990).
- ⁵⁷ Animated versions of Figs. 5, 6, 7, 8, 11, and 12 can be viewed, respectively, at <http://www.youtube.com/watch?v=818YVFHs74>, <http://www.youtube.com/watch?v=oqbFsEimi3s>, <http://www.youtube.com/watch?v=q5bmSS3VnaQ>, <http://www.youtube.com/watch?v=Fz9XKbLZbkE>, <http://www.youtube.com/watch?v=EjNVeweo0oA>, and <http://www.youtube.com/watch?v=P2ytkyuzFcA>. The animations show the same data as is reported in the associated figure; each frame of the movie represents a different value of $|\Delta/t|$, specifically each subsequent frame represents an increment of 0.1 in $|\Delta/t|$.
- ⁵⁸ G. Kotliar and D. Vollhardt, *Phys. Today* **57**, 53 (2004).
- ⁵⁹ J. Merino and R.H. McKenzie, *Phys. Rev. B* **62**, 2416 (2000).
- ⁶⁰ B. J. Powell and R. H. McKenzie, *J. Phys.: Condens. Matter*, **18**, R827, (2006).
- ⁶¹ J. Merino and R. H. McKenzie, *Phys. Rev. B* **61**, 7996 (2000).
- ⁶² P. A. Lee and N. Nagaosa, *Phys. Rev. B* **46**, 5621 (1992).
- ⁶³ A. Liebsch, *Europhys. Lett.* **63**, 97 (2003); *Phys. Rev. Lett.* **91**, 226401 (2003); *Phys. Rev. B* **70**, 165103 (2004); *Phys. Rev. Lett.* **95**, 116402 (2005); A. Koga, N. Kawakami, T. M. Rice, and M. Sigrist, *Phys. Rev. Lett.* **92**, 216402 (2004); R. Arita and K. Held, *Phys. Rev. B* **72**, 201102(R) (2005); M. Ferrero et al., *Phys. Rev. B* **72**, 205126 (2005); L. de'Medici, A. Georges, and S. Biermann, *Phys. Rev. B* **72**, 205124 (2005); M. Ferrero, F. Becca, M. Fabrizio, and M. Capone, *Phys. Rev. B* **72**, 205126 (2005); A. Rüegg, M. Inderland, S. Pilgram, and M. Sigrist, *Eur. Phys. J. B.* **48**, 55 (2005); K. Inaba and A. Koga, *Phys. Rev. B* **73**, 155106 (2006); P. G. J. van Dongen, C. Knecht, and N. Blümer, *Phys. Status Solidi (b)* **243**, 116 (2006); T. A. Costi and A. Liebsch, *Phys. Rev. Lett.* **99**, 236404 (2007); N. Blümer et al., *J. Magn. Magn. Mater.* **310**, 922 (2007); K. Bouadim, G. G. Batrouni, and R. T. Scalettar, *Phys. Rev. Lett.* **102**, 226402 (2009).
- ⁶⁴ See, for example, K. Held, A. K. McMahan, and R. T. Scalettar, *Phys. Rev. Lett.* **87**, 276404 (2001).
- ⁶⁵ V. I. Anisimov, I. A. Nekrasov, D. E. Kondakov, T. M. Rice, and M. Sigrist, *Eur. Phys. J. B.* **25**, 191 (2002); S. Nakatsuji and Y. Maeno *Phys. Rev. Lett.* **84** 2666 (2000).
- ⁶⁶ M. Ferrero, P. S. Cornaglia, L. De Leo, O. Parcollet, G. Kotliar, A. Georges, *Phys. Rev. B* **80**, 064501 (2009).

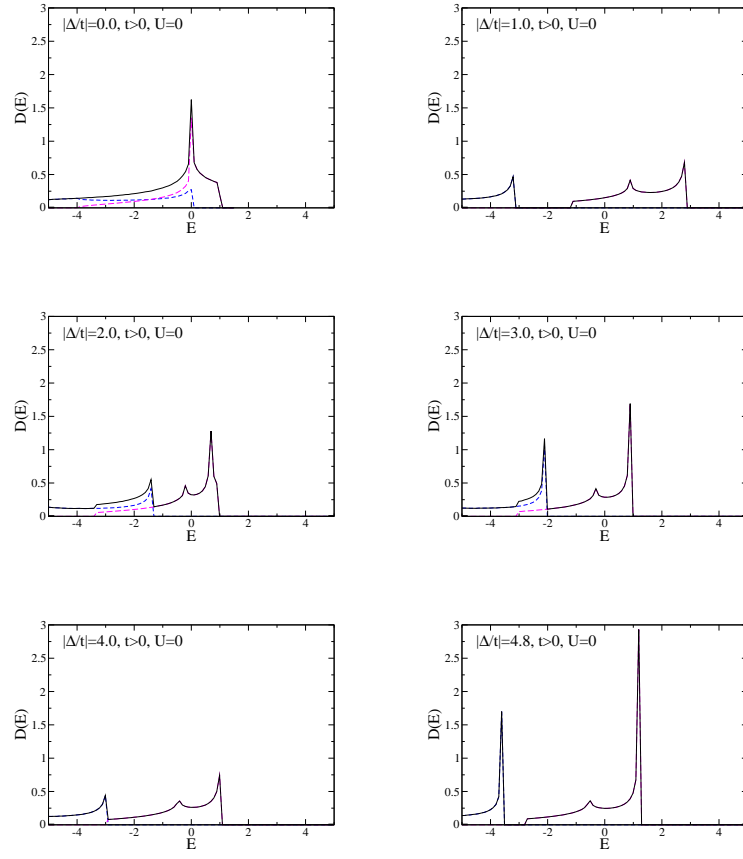


FIG. 19: [Color online] Density of states for $U = 0$ and $t > 0$. Dashed (blue and pink) lines indicate the contributions of the individual bands.